Gallionellaceae in rice root plaque: metabolic roles in iron oxidation, nutrient cycling, and plant interactions

Clara S. Chan[1,2,3,4*], Gretchen E. Dykes[3,4,5^], Rene L. Hoover[1,3,4], Matt A. Limmer[5], Angelia L. Seyfferth[1,5*]

1 Dept. of Earth Sciences, University of Delaware, Newark, DE

2 School of Marine Science and Policy, University of Delaware, Newark, Delaware, USA

3 Microbiology Graduate Program, University of Delaware, Newark, DE

4 Delaware Biotechnology Institute, Newark, DE

5 Dept. of Plant and Soil Sciences, University of Delaware, Newark, DE

*corresponding authors cschan@udel.edu, angelias@udel.edu

^current address: U.S. Environmental Protection Agency, 1200 Pennsylvania Avenue NW, Washington, DC 20004

Running title: Gallionellaceae Fe oxidizers in rice root iron plaque

Abstract

On the roots of wetland plants such as rice, iron oxidation forms iron-rich plaques that modulate plant nutrient and metal uptake. An enduring question is whether microbes catalyze this iron oxidation and, furthermore, if these iron-oxidizers mediate other important biogeochemical and plant interactions. To investigate this, we studied the microbial communities, metagenomes, and geochemistry of iron plaque on field-grown rice, as well as the surrounding rhizosphere and bulk soil. Plaque iron content (per mass root) increased over the growing season, showing continuous deposition. Analysis of 16S rRNA genes showed abundant iron-oxidizing and iron-reducing bacteria (FeOB and FeRB) in plaque, rhizosphere, and bulk soil. FeOB were enriched in plaque, suggesting FeOB affinity for the root surface. Gallionellaceae FeOB *Sideroxydans* were enriched during the vegetative and early reproductive rice growth stages, while a *Gallionella* was enriched during reproduction through grain maturity, suggesting distinct FeOB niches over the rice life cycle. FeRB *Anaeromyxobacter* and *Geobacter* increased in plaque later, during reproduction and grain ripening, corresponding to increased plaque iron. Metagenome-assembled genomes revealed that the Gallionellaceae may grow mixotrophically using both Fe(II) and organics. The *Sideroxydans* are facultative, able to use non-Fe substrates, which may allow colonization of rice roots early in the season. FeOB genomes suggest adaptations for interacting with plants, including colonization, immunity, utilization of plant organics, and nitrogen fixation. Together, our results strongly suggest that rhizoplane and rhizosphere FeOB are specifically associated with the rice plants, catalyzing the formation of iron plaque, with the potential to contribute to plant growth.

Importance

In waterlogged soils, iron plaque forms a reactive barrier between the root and soil, collecting phosphate and metals such as arsenic and cadmium. It is well established that iron-reducing bacteria solubilize iron, releasing these associated elements. In contrast, microbial roles in plaque formation have not been clear. Here we show that there is a substantial population of iron oxidizers in plaque, and furthermore, that these organisms (*Sideroxydans* and *Gallionella*) are distinguished by genes for plant colonization and nutrient fixation. Our results suggest that Fe-oxidizing and Fe-reducing bacteria form and remodel iron plaque, making it a dynamic system that represents both a temporary sink for elements (P, As, Cd, C, etc.) as well as a source. In contrast to abiotic iron oxidation, microbial iron oxidation results in coupled Fe-C-N cycling, as well as microbe-microbe and microbe-plant ecological interactions that need to be considered in soil biogeochemistry, ecosystem dynamics, and crop management.

Introduction

Iron cycling is a key biogeochemical process in rice paddies that plays important roles in the growth and quality of rice crops. Iron oxidation leads to the production of iron oxyhydroxides, which are strong sorbents of organic carbon, phosphate, and metal(oid)s such as As and Cd (1–5); iron reduction dissolves the oxyhydroxides and releases sorbed nutrients and toxins (6). Of particular interest are iron oxyhydroxide coatings (plaques) that develop on the surface of rice roots (rhizoplane), as well as in the rhizosphere (satellite plaque). Because plaque is closely associated with the plant, its formation and dissolution may drive plant uptake of oxyhydroxide-sorbed chemicals (7–10), motivating us to study mechanisms of plaque formation.

Iron-oxidizing bacteria (FeOB) can catalyze formation of iron oxyhydroxides via their metabolism. FeOB have been detected in paddy soil (10–12), making them a potential mechanism for iron plaque formation in conditions in which they can outcompete abiotic Fe oxidation.

The rice rhizoplane is in fact an ideal niche for microaerophilic FeOB, which gain energy by coupling Fe(II) oxidation to oxygen reduction, and thus grow best where Fe(II) and O_2 fluxes are high. Rice paddy soil is rich in Fe(II) formed by microbial respiration of organic matter coupled to Fe(III) reduction, thus plaque formation is partially dependent on activities of FeRB. Rice root aerenchyma are conduits of O_2, which diffuses from roots into saturated soil rich in Fe(II), providing both electron donor and acceptor for FeOB. Aerobic FeOB must compete with abiotic oxidation, and kinetics studies show they become the dominant mechanism of iron oxidation as oxygen concentrations decrease (13, 14). Different neutrophilic FeOB can thrive at O_2 concentrations <1-100 μM (15–18), concentrations that coincide with ranges typically found at the surface of rice roots (few micromolar to tens of micromolar O_2) (19, 20). Thus, it is plausible that a significant proportion of plaque iron oxidation is microbial.

Indeed, studies have increasingly documented FeOB in rice paddy soil, thus increasing recognition that microbes can contribute to iron oxidation in this environment. FeOB can be documented by culturing, 16S rRNA gene analyses, and metagenomic studies, which give different evidence of potential contributions. Numerous studies have shown that FeOB can be cultured from rice paddy soil, with a range of taxa represented (12, 18, 21–25). While culturing demonstrates microbial iron oxidation activity, it only proves that soil-derived organisms are capable of iron oxidation, but cannot show that these FeOB represent the major active organisms *in situ*. Studies using 16S rRNA genes give a broader view of soil microbial communities, but it

is often unclear which organisms are FeOB, or identification is equivocal due to the metabolic flexibility of putative FeOB. The exceptions are taxa specifically known for iron oxidation, like Gallionellaceae iron-oxidizing genera, including *Gallionella*, *Ferrigenium*, and *Sideroxydans* (22, 26, 27). As their primary metabolism is iron oxidation, detection of Gallionellaceae FeOB in field samples is a strong indication of microbial iron oxidation in the environment.

Gallionellaceae FeOB have been cultured from paddy soil, including the isolates *Gallionella/Ferrigenium kumadai* An22 (22, 28) and *Sideroxydans* sp. (18). While the isolate An22 was named *Ferrigenium* based on 16S rRNA gene dissimilarity from *Gallionella*, subsequent full-genome analyses showed that it is a *Gallionella* (29). Gallionellaceae have also been identified using 16S rRNA gene analyses including universal and taxa-specific primers in paddy soil and the rice rhizosphere (25, 30–33). Their abundance has been shown to correspond to iron oxidation in paddy soil and soil incubations (24, 34). However, it has not been shown whether Gallionellaceae are specifically enriched at the rhizoplane (vs. soil) and associated with plaque oxyhydroxides. Schmidt and Eickhorst (2014) used CARD-FISH to show Betaproteobacteria (which includes Gallionellaceae) on root surfaces, and suggested that these may represent Gallionellaceae detected via 16S rRNA sequences (35). In all, there is strong evidence for the existence of these FeOB in paddy soil, but it is still unclear if Gallionellaceae are specifically associated with plaque and therefore contribute to iron oxyhydroxide formation. If FeOB are in fact associated with plaque, this close association with the root could cause them to compete with the plant for nutrients like N, or alternatively, FeOB may provide nutrients to help promote plant growth. To understand the biogeochemical cycling in the rice root rhizosphere, we need to determine the dynamics and functions of plaque microorganisms, and their interactions with the rice plant.

102 In this study, we investigated the spatial and temporal dynamics of rice-associated FeOB
103 and FeRB in rice paddies over a growing season, using 16S rRNA gene analyses of bulk soil,
104 rhizosphere, and plaque samples. This was coupled to plaque Fe analyses as well as examination
105 of metagenomic-assembled genomes of FeOB to more specifically identify metabolic
106 capabilities and niche. Together, this allowed us to identify the major FeOB enriched in iron
107 plaque and gives insight into how microbes contribute to plaque formation over the life cycle of
108 field-grown rice.

109 Results and discussion

110 Plaque Fe content and mineralogy

111 We measured plaque Fe content on root samples obtained from 12 rice paddies at five
112 timepoints over the growing season. Plaque Fe was quantified as dithionite-citrate-bicarbonate
113 (DCB)-extractable Fe per dry root mass, obtained from one plant per paddy at each time point.
114 The amount of plaque Fe per dry root mass increased over time, with the highest rate of plaque
115 increase between heading to grain maturity (71-88 days past transplant (DPT) and 88-98 days
116 DPT, **Fig. 1a**). The increase in plaque Fe is not a function of increasing Fe in porewater, as
117 dissolved Fe(II) did not increase over time (**Fig. 1b**). The continuous increase of plaque Fe over
118 time shows active formation of plaque throughout the growing season.

119 On initial precipitation, iron oxyhydroxide minerals tend to be poorly crystalline phases
120 like ferrihydrite, later increasing in crystallinity as they age. Thus, to evaluate the potential for
121 active plaque formation, we assessed mineral composition of iron plaque at harvest (98 DPT;
122 dataset from (36)). The iron plaque mineral composition at harvest was primarily ferrihydrite,

123 with the plaque ranging from 38.6%-65.7% ferrihydrite (average 55.9%), followed by goethite
124 (21.8-37.7%, average 29.4%) (**Fig. 1c**). These results are consistent with previous observations
125 that ferrihydrite is the most abundant iron plaque mineral in rice plants at harvest (7, 9, 37–40),
126 and other wetland plants (41, 42) with goethite as a substantial proportion (9, 37, 38, 40–43).
127 While presence of ferrihydrite in the plaque at harvest is consistent with active plaque
128 formation until harvest, ferrihydrite minerals are sometimes stabilized by organics (e.g. root
129 exudates) or inorganic ions (e.g. silicon), which are present in the soil solution throughout the
130 growing season (7, 44, 45). Here, nine out of twelve paddies were amended with additional
131 silicon in various forms while three control paddies (nos. 1, 9 and 10) had no silicon added.
132 Silicon addition is known to retard the crystallization of ferrihydrite to higher ordered phases
133 (44, 46). Although plaque from the control paddies generally had lower ferrihydrite than the
134 others at harvest, ferrihydrite still comprised at least 38% of the Fe mineral composition in
135 plaque at harvest, even in controls. When considered together, increasing plaque Fe and
136 ferrihydrite in the plaque at harvest, regardless of treatment, imply active precipitation of Fe
137 oxyhydroxides over the course of the growing season.

138 Assessing the Fe-cycling microbial community by 16S rRNA gene analyses

139 FeOB and FeRB in iron plaque

140 We assessed the community composition using the 16S rRNA gene V4-V5 region. We
141 sampled bulk soil, rhizosphere soil, and Fe plaque from 12 rice paddy plots over the course of
142 one growing season (5 time points). In total, we analyzed 130 samples, from which we retrieved
143 a total of 37,072,594 quality-filtered sequences, with rarefaction analysis showing sufficient
144 sequencing depth (**Fig. S1**). The sequences clustered into 11,678 operational taxonomic units

(OTUs, 97% similarity), of which 3,914 were assigned taxonomy to the genus level (**Table S1**), from which we could predict FeOB and FeRB.

Here, we focus on organisms in the Fe plaque. To determine the most abundant plaque community members, we ranked the OTUs by their median relative abundance in the plaque (**Fig. 2a**) and looked for iron cycling organisms (**Table S2**). Twelve OTUs had median abundances greater than 0.5%, including two FeOB OTUs. The most abundant plaque OTU (OTU7) was initially identified as Gallionellaceae, and a BLAST search showed 100% identity to *Gallionella/Ferrigenium kumadai*, an FeOB that was isolated from rice paddy soil (22); hereafter, OTU7 is referred to as *Gallionella*. The third most abundant plaque OTU (OTU2) has 100% identity to a number of sequences, including *Sideroxydans* clones from riparian wetlands (acc. nos. JQ060114, JQ060109, JQ060108; (47)) and sequences from rice paddy soil (AB657736; (48)). *Sideroxydans* is a well-characterized FeOB within the *Gallionellaceae*, and has previously been cultured from rice paddies (49) and wetland plant roots (50).

The top OTUs also include several FeRB, including two *Anaeromyxobacter* OTUs, a *Geobacter*, and a *Geothrix* OTU, all of which have been previously identified in paddy soils (51–54). The second most abundant OTU was *Anaeromyxobacter* OTU0, which had 100% identity to an organism in a rice paddy soil enrichment (acc. no. MF547866; (55)). The *Geobacter* and *Geothrix* OTUs were also related to sequences from rice paddy soils (OTU6 100% to MF968163, OTU5 100% to KY287536).

In addition to iron-cycling organisms, the highly abundant plaque community members included one methylotroph (*Methylotenera* OTU37) and known cellulose degraders (*Spirochaetaceae* OTU3 and *Fibrobacterales* OTU14, (56–58). Beyond the top 12 OTUs, there were many other iron cycling OTUs, with a notable diversity of FeRB, including 32

Anaeromyxobacter and 32 *Geobacter* OTUs detected in plaque. This contrasted with three Gallionellaceae OTUs, suggesting a greater range of iron-reducing niches, despite the comparable abundance of FeOB and FeRB in plaque.

Enrichment of iron-cycling microbes in the plaque

If FeOB or FeRB are involved in plaque formation, we would expect to see them specifically enriched in plaque compared to bulk soil, and possibly also enriched in the rhizosphere. The FeOB and FeRB OTUs were generally present in all sampled biospheres: bulk, rhizosphere, and plaque. Thus, we were able to calculate an enrichment factor as the ratio of relative abundance in plaque versus bulk soil or rhizosphere versus bulk soil (**Fig. 3)**.

While there was always an FeOB enriched in the plaque, different FeOB OTUs dominated over the growth cycle. The FeOB *Sideroxydans* OTU2 was enriched at earlier time points (**Fig. 3**). *Sideroxydans* OTU2 was most enriched at the first time point (20 DPT), at 10x relative abundance in plaque, relative to bulk soil. *Sideroxydans* OTU2 was still enriched in plaque at early reproduction (42 DPT), but continued to decrease in plaque while increasing in bulk soil (**Fig. 4a**). In contrast, *Gallionella* OTU7 is most abundant and enriched in plaque at grain maturity (98 DPT) at 8x bulk soil abundance, though it was also enriched at early reproduction in the rhizosphere (42 DPT) (**Fig. 3, Fig. 4b**). These contrasting enrichment and abundance patterns suggest that *Sideroxydans* and *Gallionella* have different niches, and that *Gallionella* may be more responsive as the rice roots develop. In all, FeOB are abundant at all time points, and there is always one FeOB enriched in plaque at all times, consistent with iron oxidizer roles in plaque formation.

In contrast to FeOB, the FeRB OTUs are initially low and increase in plaque over time, in both relative abundance (**Fig. 4**) and enrichment factor (**Fig. 3**). Both of the top two FeRB OTUs,

Anaeromyxobacter OTU0 and *Geobacter* OTU6 are more abundant in the bulk soil at earlier time points (**Fig. 4c, 4e**). *Geobacter* OTU6 later becomes enriched in the plaque (12x bulk) at heading (71 DPT), while *Anaeromyxobacter* OTU0 is most abundant at grain maturity (98 DPT, 4x bulk). *Anaeromyxobacter* OTU13 and *Geothrix* OTU5 are similar to *Geobacter* OTU6 in that they peak in plaque at heading (71 DPT) (**Fig. 3, Fig. 4d, 4f**). While all the major FeRB tend to increase and become enriched in plaque over time, the different patterns suggest that there are distinct FeRB niches.

Both FeOB and FeRB are also enriched in the rhizosphere (Fig. 3, Fig. 4). Although the timing and magnitude of enrichment differs somewhat from plaque, the enrichment suggests that these organisms, particularly the FeOB, could also be associated with iron oxyhydroxide formation in the rhizosphere (satellite plaque).

Correlations between FeOB, FeRB, and plaque iron

Both FeOB and FeRB were consistently enriched and abundant in the plaque. To better understand their relationships with iron geochemistry, we looked for correlations between predominant plaque organisms and plaque Fe (**Fig. 5, Fig. S2**). Plaque Fe content was positively correlated with the relative abundance of the top FeOB *Gallionella* OTU7 (rho=0.47, p=0.09, **Fig. 5c**) and top FeRB *Anaeromyxobacter* OTU0 (rho=0.53, p=0.05, **Fig. 5a**). Because the data are from 12 paddies that vary in geochemistry, we also plotted trends within individual paddies in **Fig. 5b and 5d**. In cases where data were available for multiple time points in specific paddies, the relative abundance of both *Gallionella* OTU7 and *Anaeromyxobacter* OTU0 corresponded to higher plaque Fe in each paddy.

FeOB genomes reconstructed from rhizosphere and bulk soil metagenomes

To investigate the metabolic capabilities of FeOB, we sequenced two metagenomes from bulk soil (9BB) and rhizosphere (9BH), which were sampled from the same paddy in the same year at early reproduction (42 DPT). Based on our 16S rRNA gene analyses, these two samples include all major FeOB and FeRB OTUs, and indeed, both metagenomes yielded high quality genomes of FeOB and FeRB (>90% completeness, <5% contamination), summarized in **Table 1**. Here we briefly describe the FeRB and then focus on analyses of FeOB to assess their potential metabolic influences on biogeochemical cycling as well as plant interactions.

FeRB genomes

The metagenomes yielded nine high quality FeRB genomes, which were identified as *Anaeromyxobacter*, *Geobacter*/Geobacterales, and *Rhodoferax*. While most (6 of 9) were reconstructed from the bulk soil, one genome for each FeRB taxonomic group was recovered from the rhizosphere (**Table 1**). All of these FeRB genomes contained genes for oxygen respiration: *Anaeromyxobacter* and *Rhodoferax* genomes all encoded genes for both aa_3- and cbb_3-type cytochrome *c* oxidases while the *Geobacter* encoded either aa_3 or cbb_3 types. This indicates that all of the FeRB are facultative anaerobes.

Rhodoferax is known as an FeRB, but there is one recent report of Fe oxidation by *Rhodoferax* MIZ03 ((59); 81.7% ANI with *Rhodoferax* 9BH_DT005). The *Rhodoferax* genome from the rhizosphere includes genes that may catalyze either iron oxidation or reduction. These are homologs of the outer membrane-associated decaheme cytochrome MtoA/MtrA and porin MtoB/MtrB. In the FeRB *Shewanella oneidensis*, MtrA has also been shown to both reduce iron and take up electrons from an electrode (60). In the FeOB *Sideroxydans* ES-1, MtoA is an iron oxidase (61, 62). Phylogenetic analysis of the *Rhodoferax* 9BH_DT005 MtoA/MtrA homolog

shows that it clusters with MtoA sequences from Gallionellaceae FeOB (**Figure S3**). Altogether, this suggests that there is a possibility that the rice rhizosphere *Rhodoferax* may be a facultative Fe-reducer and Fe-oxidizer.

FeOB genomes

The metagenomes yielded four high quality FeOB genomes–three *Sideroxydans* and one *Gallionella*, classified based on a synthesis of GTDB results, average amino acid identity (AAI)/average nucleotide identity (ANI) (**Supp. Table S3**), and a phylogenetic tree of concatenated ribosomal protein sequences (**Fig. 6**). The *Sideroxydans* bins from the bulk soil (9BB_43) and rhizosphere (9BH_100) are 100% identical by ANI and cluster with *Sideroxydans lithotrophicus* ES-1 (81% ANI/82% AAI). The rhizosphere genome bin 9BH_112 is closely related to the rice paddy soil isolate *Ferrigenium kumadai* An22, (90.1% ANI/91.5% AAI); however, GTDB classifies AN22 and bin 9BH_112 as *Gallionella,* which is also confirmed by our phylogenetic analysis based on 13 concatenated ribosomal protein sequences (**Fig. 6**; details in methods and Hoover, et at. 2023). Thus, going forward, we refer to bin 9BH_112 as *Gallionella* 9BH_112 with the understanding that it is closely related to *F. kumadai* An22. The unclassified Gallionellaceae 9BH_MB008 is more distant from isolates: 79.5% ANI to *Sideroxydans* ES-1, 79.4% ANI to *Ferrigenium* An22, 79.0% ANI to *Ferriphaselus* R-1. GTDB classifies 9BH_MB008 as genus “Palsa-1006,” which has no cultured representatives, and to our knowledge, this clade has not yet been described from a rice paddy environment. Our whole genome phylogenetic analysis determined that 9BH_Bin008 and the GTDB “Palsa-1006” fall within *Sideroxydans*, so we refer to this bin as *Sideroxydans* 9BH_MB008.

While none of the reconstructed Gallionellaceae genomes from 9BB or 9BH samples include 16S rRNA genes, we can use metagenomes from samples from the following year (2017)

to help connect the genomes to 16S rRNA sequences. The *Sideroxydans* genomes 9BB_43 and 9BH_100 are practically identical (99.9% ANI, 100% AAI) with another genome reconstructed from the same sampling site a year later (9GH_6), which does have a 16S rRNA gene fragment. The 9GH_6 16S rRNA gene fragment shares 98.4% identity with a representative *Sideroxydans* OTU2 16S rRNA gene fragment. In all, the phylogenetic analyses suggest that genome reconstruction yielded genomes that are representative of the major FeOB detected by 16S analyses, *Sideroxydans* OTU2 and *Gallionella* OTU7, plus one additional *Sideroxydans* genome.

FeOB energy metabolisms - electron donors and acceptors

We analyzed Gallionellaceae bins to explore the FeOB for biogeochemical contributions, including Fe, C, N, P, and S cycling. Genes and metabolisms are summarized in **Figure 7A**.

Iron oxidation. All four 9BB/9BH Gallionellaceae genomes have genes for microaerophilic iron oxidation. The genomes contain the iron oxidase gene *cyc2*, which is characteristic of most Gallionellaceae (29). They lack *mtoAB*, an outer membrane multiheme cytochrome-porin complex associated with iron oxidation in *S. lithotrophicus* ES-1 (61–63). Each genome has the potential for oxygen respiration, with at least one set of terminal oxidase genes, *ccoNOP, coxAB,* and/or *cydAB.*

Denitrification. Only *Sideroxydans* 9BH_MB008 has the potential for dissimilatory nitrate reduction, with *napAB* in its genome. The *Sideroxydans* 9BB_43 and 9BH_100 genomes encode nitrite reductase *nirS* while *Gallionella* 9BH_112 has the *nirK* nitrite reductase. These denitrification genes are not sufficient for growth using nitrate-dependent iron oxidation metabolism, though *Sideroxydans* 9BH_MB008 may be able to use denitrification for redox balance when O_2 is limiting, as posited for Zetaproteobacteria (64).

Sulfur oxidation. All bins had genes for sulfur oxidation. In particular, *Sideroxydans* 9BB_43 and 9BH_100 have genes for multiple sulfur oxidation pathways, including thiosulfate oxidation (*soxABXYZ)* and sulfide oxidation (*dsrAB/aprAB/sat*, *fccAB, sqr*). *S. lithotrophicus* ES-1 similarly has *sox* and *dsr* genes, and is able to grow by thiosulfate oxidation. Based on previous phylogenetic analysis, the DsrAB from ES-1 and the four 9BB/9BH Gallionellaceae genomes cluster with reverse DSR (rDSR) (29).

Hydrogen. All four Gallionellaceae bins have the potential for hydrogen oxidation using a variety of hydrogenase genes. All have *hoxFUYH* and *hyaAB,* while the *Sideroxydans* genomes 9BB_43 and 9BH_100 also have *hupUV* and *hybOABC.* Hydrogenase genes are common amongst FeOB (e.g. (29, 65, 66)) and other bacteria, and may play a role in providing reducing equivalents for carbon and nitrogen fixation since the Fe(II)/Fe(III) redox potential is relatively high and requires reverse electron transport to produce NADH and ferredoxin. The variety of hydrogenases implies a range of roles, which may also include growth on hydrogen as well as fermentation, with hydrogen formation serving as an electron sink (see below).

Electron transport chain. Genes for components of the rest of the electron transport chain are present including Complex III (bc1) NADH dehydrogenase, and ATPase(s). Genes for alternative complex III (ACIII) were not found in the *Sideroxydans* 9BB_43 and 9BH_100 or *Gallionella* genomes but were present in *Sideroxydans* 9BH_MB008.

Fermentation/"anaerobic" metabolism. The Gallionellaceae genomes have a number of genes associated with anaerobic metabolisms, possibly for fermentation. *Gallionella* 9BH_112 and *Sideroxydans* 9BH_MB008 both have pyruvate formate lyase, which converts pyruvate to formate and acetyl CoA. In addition, all four Gallionellaceae encode genes for pyruvate ferredoxin/flavodoxin oxidoreductase (PFOR), which would generate acetyl coA and reduced

303 ferredoxin or flavodoxin. The four genomes also encode acetyl CoA synthetase which can
304 generate ATP during the conversion of acetyl CoA to acetate. In some cases the PFOR genes are
305 adjacent to *hox* hydrogenase genes, which may be used to evolve H_2 for redox balance (e.g.
306 (67)). As these Gallionellaceae have genes for glycogen formation and usage, this altogether
307 suggests the ability to ferment glucose into acetate, which would allow energy generation for
308 survival of anaerobic conditions. It has also been shown that PFOR can be used in place of
309 pyruvate dehydrogenase under aerobic, but highly reducing conditions as cells shift toward using
310 ferredoxin-dependent enzymes, rather than NADH, with the lower redox potential ferredoxin
311 capturing more energy and reducing power (68).

312 *Summary.* Analysis of energy metabolism genes show that the Gallionellaceae genomes
313 include genes for aerobic iron oxidation as well as sulfur oxidation, hydrogen oxidation,
314 fermentation, and in some cases, denitrification. Thus, overall, the FeOB show metabolic
315 flexibility that could serve to help them survive across chemical gradients or fluctuating redox
316 conditions. The ability to use multiple substrates can provide additional energy and reducing
317 power for biosynthetic reactions such as C and N fixation.

318 **Nutrient acquisition, fixation, storage, and usage**

319 As the FeOB are closely associated with roots, they may help promote plant growth by
320 providing nutrients. To evaluate this, we looked for genes involved in the fixation, storage, and
321 release of nutrients (**Fig. 7B**). In addition, we took note of genes that suggest utilization of plant
322 exudates and polysaccharides. As Gallionellaceae are typically considered autotrophic, such
323 genes could further link these FeOB to the plant rhizosphere environment.

324 *Carbon fixation and storage.* All Gallionellaceae isolates can grow autotrophically (22,
325 26, 27, 69–71), and like these isolates, all four Gallionellaceae genomes in this study include the

Rubisco gene *rbcL* and other genes for the complete Calvin Benson Bassham pathway for carbon fixation. The genomes also include genes for glycogen formation and degradation, which allow cells to store carbon and energy.

Organic carbon utilization. While Gallionellaceae isolates are not known for heterotrophy, the 9BB and 9BH Gallionellaceae genomes contain a number of genes for organic carbon utilization, including polysaccharide degradation, and proteinases, and organic uptake. We identified carbohydrate-degrading and production genes using the DRAM software-based classification of genes according to the Carbohydrate-Active enZYmes (CAZY) Database (**Table S4**; (72)). The four genomes contain numerous genes encoding enzymes for degradation of polysaccharides, including carbohydrate esterases and many glycoside hydrolases. We also noted numerous peptidases according to the MEROPS database, also using DRAM (https://www.ebi.ac.uk/merops/). Further work will be needed to confirm the target substrates for the genes identified above. *Sideroxydans* 9BH_MB008 encodes a dicarboxylate transporter, and all four genomes encode acetate permease. Altogether these results suggest that these Gallionellaceae are able to take advantage of active C cycling in the soil/rhizosphere and utilize plant- and microbial-derived organic carbon, and therefore grow as mixotrophic FeOB (as in ref (73, 74)).

Nitrogen fixation and storage. All four Gallionellaceae genomes have nitrogen fixation genes, including key genes *nifHDK,* as well as genes to produce the nitrogen storage compound cyanophycin and the Rnf complex, which provides electrons to nitrogenase by reducing ferredoxin via NADH (75, 76). These genes are not present in all Gallionellaceae genomes, likely because nitrogen fixation is an energy-intensive process that would be difficult to support using the limited energy available from chemolithoautotrophic iron oxidation. However, N_2

fixation and storage would give FeOB a competitive advantage at the root surface, as the cells could help supply the plant with fixed nitrogen. Past work has shown that N fixation occurs in flooded paddies mainly at the heading stage in rice (77, 78), which coincides with when *Gallionella/Ferrigenium* OTU7 begins to increase in abundance in the plaque.

Phosphorous uptake and storage. Like all Gallionellaceae, the four 9BB and 9BH FeOB genomes have genes to take up inorganic phosphate. They also have genes for polyphosphate formation and utilization, allowing them to store phosphate. This storage would be useful as dissolved phosphate levels near the root may fluctuate as phosphate is adsorbed onto iron plaque. The four FeOB genomes also include a number of genes with annotations associated with organic phosphorous utilization, but a full pathway was not observed. Thus, there may be the potential for the FeOB to use organic phosphorous sources, but this is yet to be confirmed.

What genes suggest these FeOB are specific to rice paddy soil and the root environment?

Because plaque is formed at the root surface, any plaque-forming microbes must occupy the rhizoplane and interact directly with plant roots. The Gallionellaceae genomes include various genes that could be involved in colonization and attachment to roots (**Fig. 7C**). The *Gallionella* 9BH_112 genome includes a number of adhesion genes that suggest direct interactions with the plant root. *Gallionella* 9BH_112 has genes for the "widespread colonization island" that encodes for Tad/Flp pilin, which is responsible for tight attachment to surfaces. This includes flp-1, which encodes the structural component of the pilin as well as genes to secrete the pilin and assemble the pilus. These pili mediate surface adherence and biofilm formation, and have been shown to be important for colonization (79).

Another adhesive pilin, the mannose-sensitive hemagglutination (MSHA) pilin cluster, is encoded by *Sideroxydans* 9BB_43 and 9BH_100 and *Gallionella* 9BH_112. MSHA is involved

372 in virulence in vibrio (80) and has also been shown to mediate non-virulent attachment of
373 *Pseudoalteromonas tunicata* to the green alga *Ulva australis* (81). The *Gallionella* 9BH_112
374 genome also encodes a large (3638 aa) haemagglutinin-like protein adjacent to a gene encoding a
375 hemolysin activation/secretion protein. The homologs in *Bordetella pertussis* encode FhaC, an
376 outer membrane transporter, which secretes FhaB, a filamentous haemagglutinin that mediates
377 adhesion to host tissues (82).

378 The various adhesion mechanisms would enable attachment to roots. After this initial
379 attachment, the FeOB cells would form biofilms. The genomes include a variety of genes to help
380 build biofilms, including polysaccharide synthesis. Notably, *Gallionella* 9BH_112 encodes
381 cellulose synthase, and cellulose fibrils are known to aid in *Rhizobium* and *Agrobacterium* cell
382 attachment to roots (83). *Gallionella* 9BH_112 and two *Sideroxydans* genomes 9BB_43 and
383 9BH_100 also encode a number of genes associated with capsular polysaccharide synthesis.

384 Colonization also requires the microbes to overcome plant immunity defenses. The
385 *Sideroxydans* genomes 9BH_43 and 9BH_100 both include a gene encoding alpha 2
386 macroglobulin, a protease inhibitor that is a factor in virulence and colonization (84). The alpha
387 2 macroglobulin gene is adjacent to a penicillin-binding protein 1c, similar to *Salmonella*
388 *enterica* ser. typhimurium and other bacteria. These two are thought to work together, with alpha
389 2 macroglobulin inhibiting proteases when cell walls are ruptured while the penicillin-binding
390 protein repairs cell wall peptidoglycan (84). Plants produce polyphenols, which are toxic to
391 bacteria (85); all four genomes encode polyphenol oxidases which help defend against these
392 antimicrobial compounds.

393 Other genes that may be involved in interactions with plants and other rhizosphere
394 microbes include genes for antibiotics, and toxin/antitoxins. In all, the Gallionellaceae FeOB

appear to be well-equipped to colonize plant roots, deploy immunity or antibiotic defenses as needed, contribute nutrients to plants, and utilize plant exudates in their own nutrition.

Conclusions and Implications

Our overall goal was to determine whether iron-oxidizing bacteria are associated with iron plaque and gain insight into their metabolism, dynamics, and potential plant interactions, toward understanding FeOB roles in plaque formation. In contrast to iron reduction, microbial iron oxidation is often an invisible process in the environment because abiotic processes can also oxidize Fe(II) and it can be difficult to distinguish biotic and abiotic effects. However, it is important to do so because microbial iron oxidation also drives C, N and P cycling and potentially plant processes. Here we reveal the dynamics of FeOB and FeRB in rice root plaque and rhizosphere across an entire growing season. We show that Gallionellaceae, which are well-known chemolithotrophic FeOB, are specifically enriched in both plaque and rhizosphere microbial communities and have the genetic potential to aerobically oxidize Fe(II), cycle nutrients, colonize roots, and contribute to plant nutrition.

We detected at least two different Gallionellaceae; 16S rRNA gene analyses revealed that *Sideroxydans* dominated early in the season while a *Gallionella* related to *Ferrigenium* increased over time, as plaque increased. Genomics revealed an additional, phylogenetically distinct *Sideroxydans* (9BH_MB008) that was not distinguished during 16S analyses. Both the temporal dynamics and the coexistence of the different Gallionellaceae suggest distinct niches. *Sideroxydans* are facultative iron oxidizers, shown to grow on other substrates such as thiosulfate (62, 86) and H_2 (74). At the same time, there are signs that *Sideroxydans* are primarily FeOB, as *S. lithotrophicus* ES-1 highly expresses iron oxidation genes during thiosulfate oxidation (62). The *Sideroxydans* may use their alternate (non-Fe) energy metabolisms to thrive and create

biomass in low Fe conditions, putting them in position to quickly colonize rice roots early in the season.

Gallionellaceae are known as chemolithoautotrophs, but they are commonly found in soils and sediments, and have been found to thrive in organic-rich environments like wetlands/fens (27, 87–89). Accordingly, Gallionellaceae, including the rice paddy genomes in this study, have genes for organic uptake and utilization, i.e. heterotrophy. This suggests that Gallionellaceae in fact can grow mixotrophically using both Fe and organics, taking advantage of plant exudates as a carbon source. The rice paddy Gallionellaceae have genes that further suggest a specific niche at the root surface, as they have genes for plant interactions, including colonization, immunity, uptake/utilization of plant organics, and nutrient fixation. *Gallionella* 9BH_112 is especially rich in these genes, which may explain why it increases in relative abundance as the plant matures and root mass increases. Plants are more likely to tolerate root-associated microbes that help promote plant growth, and indeed, the FeOB could provide nutrition to the rice plants. All of the Gallionellaceae genomes encode nitrogen fixation, which is otherwise a relatively unusual trait in the Gallionellaceae (< 20% of other Gallionellaceae genomes; (29)). As N fixation is an energy-intensive process, this further supports the specificity to the paddy soil environment, as Gallionellaceae have the capacity to contribute to plant nutrition and growth. Our work shows that the rhizoplane/rhizosphere hosts these microaerophilic FeOB, whose activity can produce iron oxyhydroxides. The increasing relative abundance corresponds to increasing oxyhydroxides, and thus in total, the evidence suggests these Gallionellaceae FeOB are specifically suited to the rhizosphere/rhizoplane niche and very likely contribute to plaque formation.

Alongside the FeOB, we also find FeRB enriched in the plaque, and both FeOB and FeRB increase in relative abundance over time. While it may be surprising that FeRB would occupy the aerobic zone and increase over time as oxygen levels increase, the FeRB appear to be aerotolerant, and it makes sense that FeRB would increase with increasing iron oxyhydroxide. This suggests an active iron cycle within the plaque, as well as the rhizosphere and bulk soil, where both FeOB and FeRB are also found. The production of iron plaque is likely due to the concerted action of both oxidizers and reducers, as follows. In the more reducing bulk soil, iron reduction coupled to oxidation of organics fuels the formation of dissolved Fe^{2+}. Mass flow toward the roots pulls the Fe^{2+} into the more oxic rhizosphere and root surface, where FeOB catalyze Fe^{2+} oxidation to Fe(III) oxyhydroxides. The coexistence of FeOB and FeRB suggest further redox cycling, and continued oxidation and reduction that results in dynamic remodeling of rhizosphere and rhizoplane oxyhydroxides (i.e. plaque). Thus, the formation of plaque requires *both* reducing and oxidizing conditions, and *both* FeOB and FeRB. This dynamic redox conceptual model has implications for oxyhydroxide-associated elements, and therefore plant interactions with elements like P and As. While oxyhydroxides may collect and temporarily sequester phosphate and arsenate, iron reduction in the plaque will release these elements, with consequent impacts on plant health and food safety. Further temporal studies will be needed to determine if iron-cycling dynamics within rice root plaque ultimately cause greater uptake of phosphorous and metals into plant and grain. However, this work suggests the rapid iron redox cycling between FeOB and FeRB could contribute to the plaque behaving as a dynamic source of nutrients and contaminants.

Methods

Rice paddy experiment

Samples for microbial and geochemical analyses were collected from the University of Delaware Rice Information, Communication, and Education (RICE) Facility in 2016, described by (37) and (36), and in 2017. In brief, rice (*Oryza sativa* L. 'Jefferson') was grown each year in 12, 2 x 2 m mesocosms (49 plants per paddy) that contained non-amended soil or soil amended with Si at identical Si loading rates of 5 Mg Si/ha with either rice husk, charred rice husk, or calcium silicate/silicic acid as the Si source (3 replicate paddy mesocosms per treatment). Paddies were amended prior to planting in 2015 and did not receive further Si amendments in 2016 (37) or in 2017. Treatments had less of an impact than redox status and microhabitats on the microbial community (90, 91); therefore, the present study focused on diversity and abundance of microbes associated with Fe cycling over the rice life cycle and data are averaged across all four treatments. Prior to planting in 2016 and in 2017, only roots from the previous year were tilled into the soil and paddies were fertilized with 112 kg N/ha as urea and 135 kg K_2O/ha as KCl based on soil testing and fertility recommendations. The silty clay loam soil contained 1.9 (±0.5) g/kg acid ammonium oxalate extractable Fe and 12.0 (±1.8) g/kg dithionite-citrate-bicarbonate extractable Fe as measures of amorphous and crystalline Fe (average ± standard deviation, n=12) (92). The soil pH was 6.1 (±0.5) and the soil organic matter was 2.4 (±0.6) % as measured by loss on ignition. During growth, paddies were kept flooded at transplanting until grain maturity when paddies were drained before harvest. In 2016, paddies were drained at 96 days post transplant (DPT) and in 2017, paddies were drained at 100 DPT.

Porewater chemical analyses

Weekly porewater data for 2016 are described in detail in a separate manuscript (36). In brief, porewater samples were collected weekly from June 8th, 2016 to September 6th, 2016 with Rhizon samplers (polyethersulfone, 0.15 µm pores, Soilmoisture Equipment Corp., Goleta, CA). Porewater samples were aliquoted for colorimetric measurement of Fe(II) by the ferrozine method (93), and separate porewater samples were acidified with 2% HNO_3 prior to analysis for total Fe by ICP-OES (Thermo Iris Intrepid II XSP Duo View ICP). Because porewater sampling did not occur on the same days as microbial sampling, porewater values used for comparison are an average of the closest porewater values preceding (by no more than 7 days) and following (by no more than 7 days) the microbial sampling event, except in the case of the harvest time point (98 DPT) in which only the preceding porewater time point (96 DPT) was used. Porewater sampling dates averaged for comparison to microbial sampling events are summarized in **Table S5**.

Root and soil sampling

During transplanting in May 2016 and 2017, five seedlings for each paddy mesocosm (60 plants total per year) were individually placed into 100 µm pore-size nylon mesh bags filled with paddy soil, according to (94) to define the rice rhizosphere. Different bag sizes were used to accommodate plant growth and were (diameter x depth) 10.2 cm x 20.3 cm for samples harvested at vegetative growth (20 days past-transplant (DPT)), 12.7 cm x 20.3 cm for early reproduction (42 DPT), and 15.2 cm x 31.8 cm for heading (71 DPT), grain ripening (88 DPT), and harvest (98 DPT). The five plants in mesh bags were randomly placed among 42 other transplanted seedlings.

To collect samples, bags were pulled from each paddy mesocosm at designated growth stages, and bulk soil was collected from the area surrounding the bag. Samples were immediately brought to the laboratory and separated into biospheres (plaque and rhizosphere) on ethanol-sterilized benchtops. Using sterilized instruments, rice roots were gently separated from the shoots. Roots were submerged in 25 mL 18 MΩ-cm sterile water (2016) or RNA later (2017) and vortexed twice to collect the rhizosphere. Bulk soil and rhizosphere samples were frozen at -20 °C until DNA extraction. Cleaned, rhizosphere-free roots were then divided into subsets, with half frozen prior to collecting the plaque, and half dried prior to DCB extraction of plaque Fe (described below). To collect the plaque for DNA extraction, thawed roots were transferred into 10 mL phosphate buffer solution and sonicated for 30 s twice (modified from (56)). Samples were centrifuged at 670 x g for five minutes to collect plaque, supernatant was decanted, and DNA was immediately extracted.

Plaque iron and mineralogical analysis

Fe plaque was characterized to examine changes in the quantity of plaque Fe over the rice life cycle and Fe mineral composition at harvest according to established protocols (7, 95). For this, roots in collected bags (described above) were subject to dithionite-citrate-bicarbonate extraction (95), and total Fe was measured via ICP-OES. At harvest, an additional subset of rhizosphere-free roots (three root masses sampled diagonally across each paddy and pooled) were sonicated in water and filtered onto 0.2 µm nitrocellulose membranes for bulk analysis of plaque Fe mineral composition via Fe X-ray absorption fine structure (EXAFS) spectroscopy according to (7). Samples were analyzed at the Stanford Synchrotron Radiation Lightsource (SSRL) on beamline 11-2. There, incident energy was calibrated by assigning the first Fe inflection point from a standard Fe foil of 7112 eV, and two Fe K-edge EXAFS spectra were

527 recorded for each sample in fluorescence with a Lytle detector. Spectra were averaged,
528 normalized, background subtracted and fit by linear combination in Athena using reference
529 spectra of known minerals found in Fe plaque including ferrihydrite, goethite, lepidocrocite, and
530 siderite. Further details regarding geochemical analysis are available in (36).

531 DNA extraction

532 For all bulk, rhizosphere, and plaque samples, DNA was extracted with the following
533 modifications to the manufacturer's instructions for the DNeasy PowerSoil DNA extraction kit
534 (Qiagen). Powerbead solution (200 µL) was removed from bead-beating tubes and replaced with
535 200 µL phenol:chloroform:isoamyl alcohol 25:24:1 (v/v/v). The protocol was followed to
536 manufacturer's specifications for the PowerSoil kit until conditions were adjusted for column
537 binding. At this step, equal parts lysate, solution C4, and 100% ethanol were homogenized and
538 loaded onto the DNA binding column. After DNA binding, the column was washed with 650 µL
539 100% ethanol, followed by 500 µL solution C5. The column was centrifuged and dried, and
540 DNA was eluted with molecular biology grade water (protocol based on personal communication
541 with a Qiagen representative).

542 16S rRNA gene sequencing and analysis

543 Samples were submitted to the Joint Genome Institute for paired-end (2 X 300) Illumina
544 MiSeq iTag sequencing of the 16S rRNA gene V4-V5 region, using primers 515F-Y and 926R
545 (96). Raw sequences were de-multiplexed, quality filtered and clustered to 97% similarity with
546 usearch, checking for chimeras, as part of the JGI pipeline. Feature tables and sequences were
547 imported into QIIME 2 (97), and additionally filtered to exclude any features with a frequency of
548 less than 10 sequences observed in the dataset that did not appear in at least two samples.

549 Taxonomy was assigned to features using the qiime2 sklearn naïve bayes feature classifier,
550 originally trained with SILVA database version 132 (https://www.arb-
551 silva.de/fileadmin/silva_databases/LICENSE.txt). An initial report of the 16S rRNA data was
552 given in reference (90). Data were imported into R (v3.6.2, (98)) and prepared for analysis using
553 phyloseq (v1.28.0, (99)) with qiime2R (v9.99.13, (100)). Differential abundance analysis was
554 assessed between plaque and bulk samples at individual timepoints using DESeq2 (101). Figures
555 were built using phyloseq, the phyloseq wrapper for vegan (v2.5-6, (102)) and ggplot2 (v3.3.2,
556 (103)).

557 **Metagenome sample selection, sequencing, and analysis**

558 For metagenome sequencing, we selected samples that had sufficient DNA and good
559 representation of major iron cycling OTUs. The data presented here are from a paired
560 rhizosphere and bulk soil sample set from 2016, 9BH and 9BB, sampled at 42 DPT from Paddy
561 9, a "control" paddy that received no silica amendments. Metagenome sequencing was also
562 performed on two rhizosphere samples from 2017, 9GH and 9IH, from Paddy 9 at 45 and 79
563 DPT. Here, these two samples are only used for linking 16S rRNA gene to the *Sideroxydans*
564 genomes, but are available for further analyses on IMG. For the 2017 samples, all field and DNA
565 extraction methods were as above, except that the rhizosphere sample was collected by vortexing
566 roots in 25 mL of RNA later.

567 Metagenome sequencing was performed at the Joint Genome Institute (JGI) using an
568 Illumina NovaSeq S4 (270 bp fragment, paired end 2x151). Initial data processing was done by
569 JGI, including read correction by bbcms v 38.86, (104), assembly by metaSPAdes v. 3.14.1
570 (105), and annotation by IMG Annotation Pipeline v.5.0.20. Initial binning was performed by
571 MetaBAT v2.15, evaluated using CheckM v1.1.3. Medium and high quality genomes

572 (>=50/90% completeness, <10/5% contamination; defined by the Genome Standards
573 Consortium; (106)) were uploaded to IMG.
574 We performed additional binning on the KBase platform using MaxBin v2.2.4
575 (kb_maxbin v1.1.1) (107), CONCOCT v.1.1 (kb_concoct v1.3.4) (108), MetaBAT2 v1.7 (kb
576 metabat v2.3.0) (109, 110), and then compared and optimized these bins using DASTool v1.1.2
577 (kb_das_tool v1.0.7) (111). Resulting genome bins were evaluated using CheckM v.1.0.18
578 (kb_Msuite v1.4.0) (112) and classified by GTDBtk v. 1.6.0 release 202 (kb_gtdbtk v1.0.0) (113,
579 114). We selected the highest quality genome of each known FeOB and FeRB taxa (>90%
580 completeness, <5% contamination) from each sample (9BB and 9BH) for further analysis (Table
581 1). Genome similarity was analyzed by computing average nucleotide identity (ANI) by FastANI
582 (115) in Kbase and average amino acid identity (AAI) by CompareM (116). We also assessed the
583 phylogeny of Gallionellaceae FeOB by creating a concatenated gene tree. Thirteen ribosomal
584 proteins (L19, L20, L28, L17, L9_C, S16, L21p, L27, L35p, S11, S20p, S6, S9) were aligned,
585 trimmed, masked to remove regions with >70% gaps, and concatenated in Geneious v.10.2.6
586 (117). A maximum likelihood tree was constructed in RAxML-NG v1.0.3 (118) with the LG+G
587 model and 500 bootstraps. Visualization and annotation of the final tree was done in iTOL (119).
588 Final Gallionellaceae classifications, as described above, used the concatenated gene tree-based
589 phylogeny and the scheme determined by Hoover et al., biorXiv/in review.
590 FeOB and FeRB bins selected for further analysis were annotated by RAST, DRAM
591 (kb_DRAM v.0.1.2) (120), and FeGenie (121). For certain genes of interest, we further
592 investigated close homologs by BLAST (122) against Uniprot database (123), by Blastp against
593 functionally characterized sequences, and evaluation of alignments for conserved functional

residues. For improved confidence in functional assignments, genomic context and synteny was evaluated in annotations, e.g. in RAST output.

To evaluate the potential function of the Rhodoferax Mto/Mtr homolog, we added the sequence to a tree of Mto and Mtr sequences from Hoover, et al. in review/preprint. The tree includes reference sequences of functionally verified MtoA, MtrA, and PioA along with additional Mto/Mtr sequences outlined by Hoover, et al. and Baker et al. (29, 124). Sequences were aligned, trimmed, and masked to remove gaps >70% in Geneious v.10.2.6 (117). A maximum likelihood tree was constructed using RAxML-NG v1.0.3 (118) with 500 bootstraps. The final tree was visualized and annotated using Iroki (125).

Data availability

16S rRNA gene sequences are deposited at JGI DOI 10.25585/1488298 (iTagger processed and raw sequences), and NCBI under accession PRJNA690162 (raw sequences). Metagenome sequences are available under NCBI Bioproject PRJNA710504 and at IMG (genome IDs 3300042876, 3300044673, 3300044712, 3300045051; same DOI as above), including metagenome bins. *[Note for review: JGI is in the process of submitting the remaining 3 of 4 metagenomes to NCBI as part of Bioprojects; metagenome bins will be added to these Bioprojects once this is done. Genome 9BH_MB008 is submitted as fasta files for review; other genome bins are available at IMG.]*

Acknowledgements

We thank the Joint Genome Institute for funding and performing sequencing. We thank our field sampling team: Patrick Wise, Kristy Northrup, Weida Wu, Ayofela Dare, Kendall McCoach, Fred Teasley, Douglas Amaral, Ruifang Hu, Alesia Hunter, Julia O'Brien, and Heather Eby. We thank Olushola Awoyemi for help with genome analyses.

This work was supported by the National Science Foundation Grant Nos. 1350580 and 1833525, USDA NIFA Grant No. 2016-67013-24846, the DENIN Environmental Fellows program, the University of Delaware Doctoral and Dissertation Fellowships, and the Preston C. Townsend Biotechnology Fellowship. Sequencing for this project was completed by the Joint Genome Institute for project ID 503349. Use of the Stanford Synchrotron Radiation Lightsource, SLAC National Accelerator Laboratory, is supported by the U.S. Department of Energy, Office of Science, Office of Basic Energy Sciences under Contract No. DE-AC02-76SF00515.

This work is not a product of the United States Government or the United States Environmental Protection Agency. The author/editor is not doing this work in any governmental capacity. The views expressed are his/her own and do not necessarily represent those of the United States or the US EPA.

References

1. Khan N, Seshadri B, Bolan N, Saint CP, Kirkham MB, Chowdhury S, Yamaguchi N, Lee DY, Li G, Kunhikrishnan A, Qi F, Karunanithi R, Qiu R, Zhu Y-G, Syu CH. 2016. Root

Iron Plaque on Wetland Plants as a Dynamic Pool of Nutrients and Contaminants, p. 1–96. *In* Advances in Agronomy. Elsevier.

2. Ye ZH, Baker AJM, Wong MH, Willis AJ. 1998. Zinc, lead and cadmium accumulation and tolerance in Typha latifolia as affected by iron plaque on the root surface. Aquat Bot 61:55–67.

3. Seyfferth AL, Limmer MA, Tappero R. 2021. A Method to Preserve Wetland Roots and Rhizospheres for Elemental Imaging. J Vis Exp 168.

4. Couture R-M, Rose J, Kumar N, Mitchell K, Wallschläger D, Van Cappellen P. 2013. Sorption of arsenite, arsenate, and thioarsenates to iron oxides and iron sulfides: a kinetic and spectroscopic investigation. Env Sci Technol 47:5652–5659.

5. Kocar BD, Herbel MJ, Tufano KJ, Fendorf S. 2006. Contrasting effects of dissimilatory iron(III) and arsenic(V) reduction on arsenic retention and transport. Env Sci Technol 40:6715–6721.

6. Pedersen HD, Postma D, Jakobsen R. 2006. Release of arsenic associated with the reduction and transformation of iron oxides. Geochim Cosmochim Acta 70:4116–4129.

7. Amaral DC, Lopes G, Guilherme LRG, Seyfferth AL. 2017. A New Approach to Sampling Intact Fe Plaque Reveals Si-Induced Changes in Fe Mineral Composition and Shoot As in Rice. 1. Environ Sci Technol 51:38–45.

8. Yamaguchi N, Ohkura T, Takahashi Y, Maejima Y, Arao T. 2014. Arsenic Distribution and Speciation near Rice Roots Influenced by Iron Plaques and Redox Conditions of the Soil Matrix. 3. Environ Sci Technol 48:1549–1556.

9. Seyfferth AL, Limmer M, Wu W. 2019. Si and Water Management Drives Changes in Fe and Mn Pools that Affect As Cycling and Uptake in Rice. 3. Soil Syst 3:58.

10. Xiao A, Li WC, Ye Z. 2020. Effects of Fe-oxidizing bacteria (FeOB) on iron plaque formation, As concentrations and speciation in rice (Oryza sativa L.). Ecotoxicol Environ Saf 190:110136.

11. Li X, Mou S, Chen Y, Liu T, Dong J, Li F. 2019. Microaerobic Fe(II) oxidation coupled to carbon assimilation processes driven by microbes from paddy soil. 11. Sci China Earth Sci 62:1719–1729.

12. Chen Y, Li X, Liu T, Li F. 2017. Microaerobic iron oxidation and carbon assimilation and associated microbial community in paddy soil. 3. Acta Geochim 36:502–505.

13. Druschel GK, Emerson D, Sutka R, Suchecki P, Luther GW. 2008. Low-oxygen and chemical kinetic constraints on the geochemical niche of neutrophilic iron(II) oxidizing microorganisms. 14. Geochim Cosmochim Acta 72:3358–3370.

14. McAllister SM, Moore RM, Gartman A, Luther GW, Emerson D, Chan CS. 2019. The Fe(II)-oxidizing *Zetaproteobacteria* : historical, ecological and genomic perspectives. FEMS Microbiol Ecol 95.

669 15. Chan CS, McAllister SM, Leavitt AH, Glazer BT, Krepski ST, Emerson D. 2016. The
670 architecture of iron microbial mats reflects the adaptation of chemolithotrophic iron
671 oxidation in freshwater and marine environments. Front Microbiol 7:796.

672 16. Chiu BK, Kato S, McAllister SM, Field EK, Chan CS. 2017. Novel Pelagic Iron-
673 Oxidizing Zetaproteobacteria from the Chesapeake Bay Oxic–Anoxic Transition Zone.
674 Front Microbiol 8.

675 17. Fleming EJ, Cetinić I, Chan CS, Whitney King D, Emerson D. 2014. Ecological
676 succession among iron-oxidizing bacteria. ISME J 8:804–815.

677 18. Maisch M, Lueder U, Kappler A, Schmidt C. 2019. Iron Lung: How Rice Roots Induce
678 Iron Redox Changes in the Rhizosphere and Create Niches for Microaerophilic Fe(II)-
679 Oxidizing Bacteria. Environ Sci Technol Lett acs.estlett.9b00403.

680 19. Larsen M, Santner J, Oburger E, Wenzel WW, Glud RN. 2015. O2 dynamics in the
681 rhizosphere of young rice plants (Oryza sativa L.) as studied by planar optodes. Plant Soil
682 390:279–292.

683 20. Revsbech NP, Pedersen O, Reichardt W, Briones A. 1999. Microsensor analysis of
684 oxygen and pH in the rice rhizosphere under field and laboratory conditions. Biol Fertil
685 Soils 29:379–385.

686 21. Chen Y, Li X, Liu T, Li F, Sun W, Young LY, Huang W. 2022. Metagenomic analysis of
687 Fe(II)-oxidizing bacteria for Fe(III) mineral formation and carbon assimilation under
688 microoxic conditions in paddy soil. Sci Total Environ 851:158068.

689 22. Khalifa A, Nakasuji Y, Saka N, Honjo H, Asakawa S, Watanabe T. 2018. Ferrigenium
690 kumadai gen. nov., sp. nov., a microaerophilic iron-oxidizing bacterium isolated from a
691 paddy field soil. 8. Int J Syst Evol Microbiol 68:2587–2592.

692 23. Liesack W, Schnell S, Revsbech NP. 2000. Microbiology of flooded rice paddies. 5.
693 FEMS Microbiol Rev 24:625–645.

694 24. Nakagawa K, Murase J, Asakawa S, Watanabe T. 2020. Involvement of microaerophilic
695 iron-oxidizing bacteria in the iron-oxidizing process at the surface layer of flooded paddy
696 field soil. J Soils Sediments https://doi.org/10.1007/s11368-020-02717-w.

697 25. Naruse T, Ban Y, Yoshida T, Kato T, Namikawa M, Takahashi T, Nishida M, Asakawa S,
698 Watanabe T. 2019. Community structure of microaerophilic iron-oxidizing bacteria in
699 Japanese paddy field soils. Soil Sci Plant Nutr 65:460–470.

700 26. Emerson D, Moyer C. 1997. Isolation and characterization of novel iron-oxidizing bacteria
701 that grow at circumneutral pH. 12. Appl Environ Microbiol 63:4784–4792.

702 27. Lüdecke C, Reiche M, Eusterhues K, Nietzsche S, Küsel K. 2010. Acid-tolerant
703 microaerophilic Fe(II)-oxidizing bacteria promote Fe(III)-accumulation in a fen: Acid-
704 tolerant Fe(II)-oxidizers in a fen. Environ Microbiol 12:2814–2825.

705 28. Watanabe T, Khalifa A, Asakawa S. 2021. Complete Genome Sequence of Ferrigenium
706 kumadai An22, a Microaerophilic Iron-Oxidizing Bacterium Isolated from a Paddy Field
707 Soil. Microbiol Resour Announc 10.

29. Hoover RL, Keffer JL, Polson SW, Chan CS. 2023. Gallionellaceae pangenomic analysis reveals insight into phylogeny, metabolic flexibility, and iron oxidation mechanisms. In review. bioRxiv https://doi.org/10.1101/2023.01.26.525709.

30. Schmidt H, Eickhorst T. 2014. Detection and quantification of native microbial populations on soil-grown rice roots by catalyzed reporter deposition-fluorescence *in situ* hybridization. 2. FEMS Microbiol Ecol 87:390–402.

31. Tang X, Zou L, Su S, Lu Y, Zhai W, Manzoor M, Liao Y, Nie J, Shi J, Ma LQ, Xu J. 2021. Long-Term Manure Application Changes Bacterial Communities in Rice Rhizosphere and Arsenic Speciation in Rice Grains. Environ Sci Technol 55:1555–1565.

32. Wang M, Tang Z, Chen X-P, Wang X, Zhou W-X, Tang Z, Zhang J, Zhao F-J. 2019. Water management impacts the soil microbial communities and total arsenic and methylated arsenicals in rice grains. Environ Pollut 247:736–744.

33. Zecchin S, Corsini A, Martin M, Cavalca L. 2017. Influence of water management on the active root-associated microbiota involved in arsenic, iron, and sulfur cycles in rice paddies. Appl Microbiol Biotechnol 101:6725–6738.

34. Watanabe T, Katayanagi N, Agbisit R, Llorca L, Hosen Y, Asakawa S. 2021. Influence of alternate wetting and drying water-saving irrigation practice on the dynamics of Gallionella-related iron-oxidizing bacterial community in paddy field soil. Soil Biol Biochem 152:108064.

35. Schmidt H, Eickhorst T. 2013. Spatio-temporal variability of microbial abundance and community structure in the puddled layer of a paddy soil cultivated with wetland rice (Oryza sativa L.). Appl Soil Ecol 72:93–102.

36. Limmer MA, Seyfferth AL. 2020. Carryover effects of silicon-rich amendments in rice paddies. Soil Sci Soc Am J saj2.20146.

37. Limmer MA, Mann J, Amaral DC, Vargas R, Seyfferth AL. 2018. Silicon-rich amendments in rice paddies: Effects on arsenic uptake and biogeochemistry. Sci Total Environ 624:1360–1368.

38. Liu WJ, Zhu YG, Hu Y, Williams PN, Gault AG, Meharg AA, Charnock JM, Smith FA. 2006. Arsenic Sequestration in Iron Plaque, Its Accumulation and Speciation in Mature Rice Plants (*Oryza Sativa* L.). 18. Environ Sci Technol 40:5730–5736.

39. Seyfferth AL, Webb SM, Andrews JC, Fendorf S. 2011. Defining the distribution of arsenic species and plant nutrients in rice (Oryza sativa L.) from the root to the grain. 21. Geochim Cosmochim Acta 75:6655–6671.

40. Teasley WA, Limmer MA, Seyfferth AL. 2017. How Rice (*Oryza sativa* L.) Responds to Elevated As under Different Si-Rich Soil Amendments. 18. Environ Sci Technol 51:10335–10343.

41. Hansel CM, Fendorf S, Sutton S, Newville M. 2001. Characterization of Fe Plaque and Associated Metals on the Roots of Mine-Waste Impacted Aquatic Plants. 19. Environ Sci Technol 35:3863–3868.

42. Hansel CM, La Force MJ, Fendorf S, Sutton S. 2002. Spatial and Temporal Association of As and Fe Species on Aquatic Plant Roots. 9. Environ Sci Technol 36:1988–1994.

43. Maisch M, Lueder U, Kappler A, Schmidt C. 2020. From Plant to Paddy—How Rice Root Iron Plaque Can Affect the Paddy Field Iron Cycling. 2. Soil Syst 4:28.

44. Jones AM, Collins RN, Rose J, Waite TD. 2009. The effect of silica and natural organic matter on the Fe(II)-catalysed transformation and reactivity of Fe(III) minerals. Geochim Cosmochim Acta 14.

45. Seyfferth AL. 2015. Abiotic effects of dissolved oxyanions on iron plaque quantity and mineral composition in a simulated rhizosphere. 1–2. Plant Soil 397:43–61.

46. Schwertmann U, Taylor RM. 1972. Influence of silicate on transformation of lepidocrocite to goethite. Clays Clay Min 20:159–164.

47. Wang J, Krause S, Muyzer G, Meima-Franke M, Laanbroek H, Bodelier P. 2012. Spatial Patterns of Iron- and Methane-Oxidizing Bacterial Communities in an Irregularly Flooded, Riparian Wetland. Front Microbiol 3.

48. Itoh H, Ishii S, Shiratori Y, Oshima K, Otsuka S, Hattori M, Senoo K. 2013. Seasonal Transition of Active Bacterial and Archaeal Communities in Relation to Water Management in Paddy Soils. Microbes Environ 28:370–380.

49. Maisch M, Lueder U, Laufer K, Scholze C, Kappler A, Schmidt C. 2019. Contribution of Microaerophilic Iron(II)-Oxidizers to Iron(III) Mineral Formation. 14. Environ Sci Technol 53:8197–8204.

767 50. Weiss JV, Rentz JA, Plaia T, Neubauer SC, Merrill-Floyd M, Lilburn T, Bradburne C,
768 Megonigal JP, Emerson D. 2007. Characterization of Neutrophilic Fe(II)-Oxidizing
769 Bacteria Isolated from the Rhizosphere of Wetland Plants and Description of
770 Ferritrophicum radicicola gen. nov. sp. nov., and Sideroxydans paludicola sp. nov.
771 Geomicrobiol J 24:559–570.

772 51. Ding L-J, Su J-Q, Xu H-J, Jia Z-J, Zhu Y-G. 2015. Long-term nitrogen fertilization of
773 paddy soil shifts iron-reducing microbial community revealed by RNA-13C-acetate
774 probing coupled with pyrosequencing. 3. ISME J 9:721–734.

775 52. Hori T, Müller A, Igarashi Y, Conrad R, Friedrich MW. 2010. Identification of iron-
776 reducing microorganisms in anoxic rice paddy soil by 13C-acetate probing. 2. ISME J
777 4:267–278.

778 53. Kouzuma A, Kasai T, Nakagawa G, Yamamuro A, Abe T, Watanabe K. 2013.
779 Comparative Metagenomics of Anode-Associated Microbiomes Developed in Rice Paddy-
780 Field Microbial Fuel Cells. 11. PLoS ONE 8.

781 54. Sun M, Xiao T, Ning Z, Xiao E, Sun W. 2015. Microbial community analysis in rice
782 paddy soils irrigated by acid mine drainage contaminated water. 6. Appl Microbiol
783 Biotechnol 99:2911–2922.

784 55. Reid MC, Maillard J, Bagnoud A, Falquet L, Le Vo P, Bernier-Latmani R. 2017. Arsenic
785 Methylation Dynamics in a Rice Paddy Soil Anaerobic Enrichment Culture. 18. Environ
786 Sci Technol 51:10546–10554.

787 56. Edwards J, Johnson C, Santos-Medellín C, Lurie E, Podishetty NK, Bhatnagar S, Eisen
788 JA, Sundaresan V. 2015. Structure, variation, and assembly of the root-associated
789 microbiomes of rice. 8. Proc Natl Acad Sci 112:E911–E920.

790 57. Ransom-Jones E, Jones DL, McCarthy AJ, McDonald JE. 2012. The Fibrobacteres: an
791 Important Phylum of Cellulose-Degrading Bacteria. 2. Microb Ecol 63:267–281.

792 58. Leschine SB. 1995. Cellulose Degradation in Anaerobic Environments. Annu Rev
793 Microbiol 49:399–426.

794 59. Kato S, Ohkuma M. 2021. A Single Bacterium Capable of Oxidation and Reduction of
795 Iron at Circumneutral pH. Microbiol Spectr 9:e00161-21.

796 60. Ross DE, Flynn JM, Baron DB, Gralnick JA, Bond DR. 2011. Towards Electrosynthesis
797 in Shewanella: Energetics of Reversing the Mtr Pathway for Reductive Metabolism. PLOS
798 ONE 6:e16649.

799 61. Liu J, Wang Z, Belchik SM, Edwards MJ, Liu C, Kennedy DW, Merkley ED, Lipton MS,
800 Butt JN, Richardson DJ, Zachara JM, Fredrickson JK, Rosso KM, Shi L. 2012.
801 Identification and Characterization of MtoA: A Decaheme c-Type Cytochrome of the
802 Neutrophilic Fe(II)-Oxidizing Bacterium Sideroxydans lithotrophicus ES-1. Front
803 Microbiol 3.

804 62. Zhou N, Keffer JL, Polson SW, Chan CS. 2022. Unraveling Fe(II)-Oxidizing Mechanisms
805 in a Facultative Fe(II) Oxidizer, Sideroxydans lithotrophicus Strain ES-1, via Culturing,
806 Transcriptomics, and Reverse Transcription-Quantitative PCR. Appl Environ Microbiol
807 88:e01595-21.

808 63. Zhou N, Kupper RJ, Catalano JG, Thompson A, Chan CS. 2022. Biological Oxidation of
809 Fe(II)-Bearing Smectite by Microaerophilic Iron Oxidizer Sideroxydans lithotrophicus
810 Using Dual Mto and Cyc2 Iron Oxidation Pathways. Environ Sci Technol
811 https://doi.org/10.1021/acs.est.2c05142.

812 64. McAllister SM, Vandzura R, Keffer JL, Polson SW, Chan CS. 2020. Aerobic and
813 anaerobic iron oxidizers together drive denitrification and carbon cycling at marine iron-
814 rich hydrothermal vents. ISME J https://doi.org/10.1038/s41396-020-00849-y.

815 65. Mori JF, Scott JJ, Hager KW, Moyer CL, Küsel K, Emerson D. 2017. Physiological and
816 ecological implications of an iron- or hydrogen-oxidizing member of the
817 Zetaproteobacteria, Ghiorsea bivora, gen. nov., sp. nov. ISME J 11:2624–2636.

818 66. McAllister SM, Polson SW, Butterfield DA, Glazer BT, Sylvan JB, Chan CS. 2020.
819 Validating the Cyc2 neutrophilic iron oxidation pathway using meta-omics of
820 Zetaproteobacteria iron mats at marine hydrothermal vents. mSystems 5:e00553-19.

821 67. Khanna N, Lindblad P. 2015. Cyanobacterial Hydrogenases and Hydrogen Metabolism
822 Revisited: Recent Progress and Future Prospects. 5. Int J Mol Sci 16:10537–10561.

823 68. Wang Y, Chen X, Spengler K, Terberger K, Boehm M, Appel J, Barske T, Timm S,
824 Battchikova N, Hagemann M, Gutekunst K. 2022. Pyruvate:ferredoxin oxidoreductase and
825 low abundant ferredoxins support aerobic photomixotrophic growth in cyanobacteria.
826 eLife 11:e71339.

69. Krepski ST, Hanson TE, Chan CS. 2012. Isolation and characterization of a novel biomineral stalk-forming iron-oxidizing bacterium from a circumneutral groundwater seep: A novel stalk-forming Fe-oxidizing bacterium. 7. Environ Microbiol 14:1671–1680.

70. Kato S, Krepski S, Chan C, Itoh T, Ohkuma M. 2014. Ferriphaselus amnicola gen. nov., sp. nov., a neutrophilic, stalk-forming, iron-oxidizing bacterium isolated from an iron-rich groundwater seep. Int J Syst Evol Microbiol 64:921–925.

71. Kato S, Itoh T, Iino T, Ohkuma M. 2022. Sideroxyarcus emersonii gen. nov. sp. nov., a neutrophilic, microaerobic iron- and thiosulfate-oxidizing bacterium isolated from iron-rich wetland sediment. Int J Syst Evol Microbiol 72.

72. Drula E, Garron M-L, Dogan S, Lombard V, Henrissat B, Terrapon N. 2022. The carbohydrate-active enzyme database: functions and literature. Nucleic Acids Res 50:D571–D577.

73. Akob DM, Hallenbeck M, Beulig F, Fabisch M, Küsel K, Keffer JL, Woyke T, Shapiro N, Lapidus A, Klenk H-P, Chan CS. 2020. Mixotrophic iron-oxidizing *Thiomonas* isolates from an acid mine drainage-affected creek. Appl Environ Microbiol 86:e01424-20.

74. Cooper RE, Finck J, Chan C, Küsel K. 2023. Mixotrophy broadens the ecological niche range of the iron oxidizer Sideroxydans sp. CL21 isolated from an iron-rich peatland. FEMS Microbiol Ecol fiac156.

75. Obst M, Steinbüchel A. 2006. Cyanophycin—an Ideal Bacterial Nitrogen Storage Material with Unique Chemical Properties, p. 167–193. *In* Shively, JM (ed.), Inclusions in Prokaryotes. Springer, Berlin, Heidelberg.

76. Schmehl M, Jahn A, Meyer zu Vilsendorf A, Hennecke S, Masepohl B, Schuppler M, Marxer M, Oelze J, Klipp W. 1993. Identification of a new class of nitrogen fixation genes in Rhodobacter capsalatus: a putative membrane complex involved in electron transport to nitrogenase. Mol Gen Genet MGG 241:602–615.

77. Bothe H, de Bruijn FJ, Newton WE. 1988. In Proceeding in Nitrogen Fixation: Hundred years after, p. 747–752. *In* In Proceeding in Nitrogen Fixation: Hundred years after. Gustav Fischer, Stuttgart, New York.

78. Ladha JK, Padre AT, Punzalan GC, Watanabe I, De Data SK. 1988. Ability of wetland rice to stimulate biological nitrogen fixation and utilize soil nitrogen.

79. Tomich M, Planet PJ, Figurski DH. 2007. The tad locus: postcards from the widespread colonization island. 5. Nat Rev Microbiol 5:363–375.

80. Fullner KJ, Mekalanos JJ. 1999. Genetic Characterization of a New Type IV-A Pilus Gene Cluster Found in Both Classical and El Tor Biotypes ofVibrio cholerae. Infect Immun 67:1393–1404.

81. Dalisay DS, Webb JS, Scheffel A, Svenson C, James S, Holmström C, Egan S, Kjelleberg S. 2006. A mannose-sensitive haemagglutinin (MSHA)-like pilus promotes attachment of Pseudoalteromonas tunicata cells to the surface of the green alga Ulva australis. Microbiology 152:2875–2883.

82. Scheller EV, Cotter PA. 2015. Bordetella filamentous hemagglutinin and fimbriae: critical adhesins with unrealized vaccine potential. Pathog Dis 73.

868 83. Knights HE, Jorrin B, Haskett TL, Poole PS. 2021. Deciphering bacterial mechanisms of
869 root colonization. Environ Microbiol Rep 13:428–444.

870 84. Wong SG, Dessen A. 2014. Structure of a bacterial α2-macroglobulin reveals mimicry of
871 eukaryotic innate immunity. 1. Nat Commun 5:4917.

872 85. Daglia M. 2012. Polyphenols as antimicrobial agents. Curr Opin Biotechnol 23:174–181.

873 86. Emerson D, Field EK, Chertkov O, Davenport KW, Goodwin L, Munk C, Nolan M,
874 Woyke T. 2013. Comparative genomics of freshwater Fe-oxidizing bacteria: implications
875 for physiology, ecology, and systematics. Front Microbiol 4.

876 87. Kügler S, Cooper RE, Wegner C-E, Mohr JF, Wichard T, Küsel K. 2019. Iron-organic
877 matter complexes accelerate microbial iron cycling in an iron-rich fen. Sci Total Environ
878 646:972–988.

879 88. Neubauer SC, Toledo-Durán GE, Emerson D, Megonigal JP. 2007. Returning to Their
880 Roots: Iron-Oxidizing Bacteria Enhance Short-Term Plaque Formation in the Wetland-
881 Plant Rhizosphere. 1. Geomicrobiol J 24:65–73.

882 89. Yang L, Jiang M, Zou Y, Qin L, Chen Y. 2021. Geographical Distribution of Iron Redox
883 Cycling Bacterial Community in Peatlands: Distinct Assemble Mechanism Across
884 Environmental Gradient. Front Microbiol 12.

885 90. Dykes GE, Chan CS, Seyfferth AL. 2021. 16S rRNA Gene Amplicon Sequencing Data
886 from Flooded Rice Paddy Mesocosms Treated with Different Silicon-Rich Soil
887 Amendments. Microbiol Resour Announc 10:e00178-21.

888 91. Dykes GE, Limmer MA, Seyfferth AL. 2021. Silicon-rich soil amendments impact
889 microbial community composition and the composition of arsM bearing microbes. Plant
890 Soil 468:147–164.

891 92. 1996. Methods of soil analysis. Part 3: Chemical methods. Soil Science Society of
892 America : American Society of Agronomy, Madison, Wis.

893 93. Stookey LL. 1970. Ferrozine---a new spectrophotometric reagent for iron. Anal Chem
894 42:779–781.

895 94. Jia Y, Huang H, Zhong M, Wang F-H, Zhang L-M, Zhu Y-G. 2013. Microbial Arsenic
896 Methylation in Soil and Rice Rhizosphere. 7. Environ Sci Technol 47:3141–3148.

897 95. Taylor GJ, Crowder AA. 1983. Use of the DCB Technique for Extraction of Hydrous Iron
898 Oxides from Roots of Wetland Plants. 8. Am J Bot 70:1254–1257.

899 96. Parada AE, Needham DM, Fuhrman JA. 2016. Every base matters: assessing small
900 subunit rRNA primers for marine microbiomes with mock communities, time series and
901 global field samples. 5. Environ Microbiol 18:1403–1414.

902 97. Bolyen E, Rideout JR, Dillon MR, Bokulich NA, Abnet CC, Al-Ghalith GA, Alexander H,
903 Alm EJ, Arumugam M, Asnicar F, Bai Y, Bisanz JE, Bittinger K, Brejnrod A, Brislawn
904 CJ, Brown CT, Callahan BJ, Caraballo-Rodríguez AM, Chase J, Cope EK, Da Silva R,
905 Diener C, Dorrestein PC, Douglas GM, Durall DM, Duvallet C, Edwardson CF, Ernst M,
906 Estaki M, Fouquier J, Gauglitz JM, Gibbons SM, Gibson DL, Gonzalez A, Gorlick K,
907 Guo J, Hillmann B, Holmes S, Holste H, Huttenhower C, Huttley GA, Janssen S,
908 Jarmusch AK, Jiang L, Kaehler BD, Kang KB, Keefe CR, Keim P, Kelley ST, Knights D,

909 Koester I, Kosciolek T, Kreps J, Langille MGI, Lee J, Ley R, Liu Y-X, Loftfield E,
910 Lozupone C, Maher M, Marotz C, Martin BD, McDonald D, McIver LJ, Melnik AV,
911 Metcalf JL, Morgan SC, Morton JT, Naimey AT, Navas-Molina JA, Nothias LF,
912 Orchanian SB, Pearson T, Peoples SL, Petras D, Preuss ML, Pruesse E, Rasmussen LB,
913 Rivers A, Robeson MS, Rosenthal P, Segata N, Shaffer M, Shiffer A, Sinha R, Song SJ,
914 Spear JR, Swafford AD, Thompson LR, Torres PJ, Trinh P, Tripathi A, Turnbaugh PJ, Ul-
915 Hasan S, van der Hooft JJJ, Vargas F, Vázquez-Baeza Y, Vogtmann E, von Hippel M,
916 Walters W, Wan Y, Wang M, Warren J, Weber KC, Williamson CHD, Willis AD, Xu ZZ,
917 Zaneveld JR, Zhang Y, Zhu Q, Knight R, Caporaso JG. 2019. Reproducible, interactive,
918 scalable and extensible microbiome data science using QIIME 2. 8. Nat Biotechnol
919 37:852–857.

920 98. R Core Team. 2019. R: A Language and Environment for Statistical Computing. R
921 Foundation for Statistical Computing, Vienna, Austria. https://www.R-project.org/.

922 99. McMurdie PJ, Holmes S. 2013. phyloseq: An R Package for Reproducible Interactive
923 Analysis and Graphics of Microbiome Census Data. 4. PLoS ONE 8:e61217.

924 100. Bisanz JE. 2018. qiime2R: Importing QIIME2 artifacts and associated data into R
925 sessions.

926 101. Love MI, Huber W, Anders S. 2014. Moderated estimation of fold change and dispersion
927 for RNA-seq data with DESeq2. 12. Genome Biol 15:550.

928 102. Oksanen J, Blanchet FG, Friendly M, Kindt R, Legendre P, McGlinn D, Minchin PR,
929 O'Hara RB, Simpson GL, Solymos P, Stevens MHH, Szoecs E, Wagner H. 2019. vegan:
930 Community Ecology Package. https://CRAN.R-project.org/package=vegan.

931 103. Wickham H. 2016. ggplot2: Elegant Graphics for Data Analysis. Springer-Verlag New
932 York. https://ggplot2.tidyverse.org.

933 104. Bushnell B. BBMap.

934 105. Nurk S, Meleshko D, Korobeynikov A, Pevzner PA. 2017. metaSPAdes: a new versatile
935 metagenomic assembler. Genome Res 27:824–834.

936 106. Bowers RM, Kyrpides NC, Stepanauskas R, Harmon-Smith M, Doud D, Reddy TBK,
937 Schulz F, Jarett J, Rivers AR, Eloe-Fadrosh EA, Tringe SG, Ivanova NN, Copeland A,
938 Clum A, Becraft ED, Malmstrom RR, Birren B, Podar M, Bork P, Weinstock GM, Garrity
939 GM, Dodsworth JA, Yooseph S, Sutton G, Glöckner FO, Gilbert JA, Nelson WC, Hallam
940 SJ, Jungbluth SP, Ettema TJG, Tighe S, Konstantinidis KT, Liu W-T, Baker BJ, Rattei T,
941 Eisen JA, Hedlund B, McMahon KD, Fierer N, Knight R, Finn R, Cochrane G, Karsch-
942 Mizrachi I, Tyson GW, Rinke C, Lapidus A, Meyer F, Yilmaz P, Parks DH, Eren AM,
943 Schriml L, Banfield JF, Hugenholtz P, Woyke T. 2017. Minimum information about a
944 single amplified genome (MISAG) and a metagenome-assembled genome (MIMAG) of
945 bacteria and archaea. 8. Nat Biotechnol 35:725–731.

946 107. Wu Y-W, Tang Y-H, Tringe SG, Simmons BA, Singer SW. 2014. MaxBin: an automated
947 binning method to recover individual genomes from metagenomes using an expectation-
948 maximization algorithm. Microbiome 2:26.

949 108. Alneberg J, Bjarnason BS, de Bruijn I, Schirmer M, Quick J, Ijaz UZ, Lahti L, Loman NJ,
950 Andersson AF, Quince C. 2014. Binning metagenomic contigs by coverage and
951 composition. 11. Nat Methods 11:1144–1146.

952 109. Kang DD, Froula J, Egan R, Wang Z. 2015. MetaBAT, an efficient tool for accurately
953 reconstructing single genomes from complex microbial communities. PeerJ 3:e1165.

954 110. Kang DD, Li F, Kirton E, Thomas A, Egan R, An H, Wang Z. 2019. MetaBAT 2: an
955 adaptive binning algorithm for robust and efficient genome reconstruction from
956 metagenome assemblies. PeerJ 7:e7359.

957 111. Sieber CMK, Probst AJ, Sharrar A, Thomas BC, Hess M, Tringe SG, Banfield JF. 2018.
958 Recovery of genomes from metagenomes via a dereplication, aggregation and scoring
959 strategy. 7. Nat Microbiol 3:836–843.

960 112. Parks DH, Imelfort M, Skennerton CT, Hugenholtz P, Tyson GW. 2015. CheckM:
961 assessing the quality of microbial genomes recovered from isolates, single cells, and
962 metagenomes. Genome Res 25:1043–1055.

963 113. Chaumeil P-A, Mussig AJ, Hugenholtz P, Parks DH. 2020. GTDB-Tk: a toolkit to classify
964 genomes with the Genome Taxonomy Database. Bioinformatics 36:1925–1927.

965 114. Chaumeil P-A, Mussig AJ, Hugenholtz P, Parks DH. 2022. GTDB-Tk v2: memory
966 friendly classification with the Genome Taxonomy Database. Bioinformatics btac672.

967 115. Jain C, Rodriguez-R LM, Phillippy AM, Konstantinidis KT, Aluru S. 2018. High
968 throughput ANI analysis of 90K prokaryotic genomes reveals clear species boundaries.
969 Nat Commun 9:5114.

970 116. Parks D. 2014. CompareM. Github repository. https://github.com/dparks1134/CompareM.

971 117. Geneious v.10.2.6. https://www.geneious.com.

972 118. Kozlov AM, Darriba D, Flouri T, Morel B, Stamatakis A. 2019. RAxML-NG: a fast,
973 scalable and user-friendly tool for maximum likelihood phylogenetic inference. 21.
974 Bioinformatics 35:4453–4455.

975 119. Letunic I, Bork P. 2021. Interactive Tree Of Life (iTOL) v5: an online tool for
976 phylogenetic tree display and annotation. Nucleic Acids Res 49:W293–W296.

977 120. Shaffer M, Borton MA, McGivern BB, Zayed AA, Rosa SLL, Solden LM, Liu P, Narrowe
978 AB, Rodriguez-Ramos J, Bolduc B, Gazitua MC, Daly RA, Smith GJ, Vik DR, Pope PB,
979 Sullivan MB, Roux S, Wrighton KC. 2020. DRAM for distilling microbial metabolism to
980 automate the curation of microbiome function. bioRxiv 2020.06.29.177501.

981 121. Garber AI, Nealson KH, Okamoto A, McAllister SM, Chan CS, Barco RA, Merino N.
982 2020. FeGenie: A comprehensive tool for the identification of iron genes and iron gene
983 neighborhoods in genome and metagenome assemblies. Front Microbiol 11:37.

984 122. Altschul SF, Gish W, Miller W, Myers EW, Lipman DJ. 1990. Basic local alignment
985 search tool. J Mol Biol 215:403–410.

986 123. The UniProt Consortium. 2021. UniProt: the universal protein knowledgebase in 2021.
987 Nucleic Acids Res 49:D480–D489.

988 124. Baker IR, Conley BE, Gralnick JA, Girguis PR. 2022. Evidence for Horizontal and
989 Vertical Transmission of Mtr-Mediated Extracellular Electron Transfer among the
990 Bacteria. mBio https://doi.org/10.1128/mbio.02904-21.

991 125. Moore RM, Harrison AO, McAllister SM, Polson SW, Wommack EK. 2020. Iroki:
992 automatic customization and visualization of phylogenetic trees.

993

Figures and Table

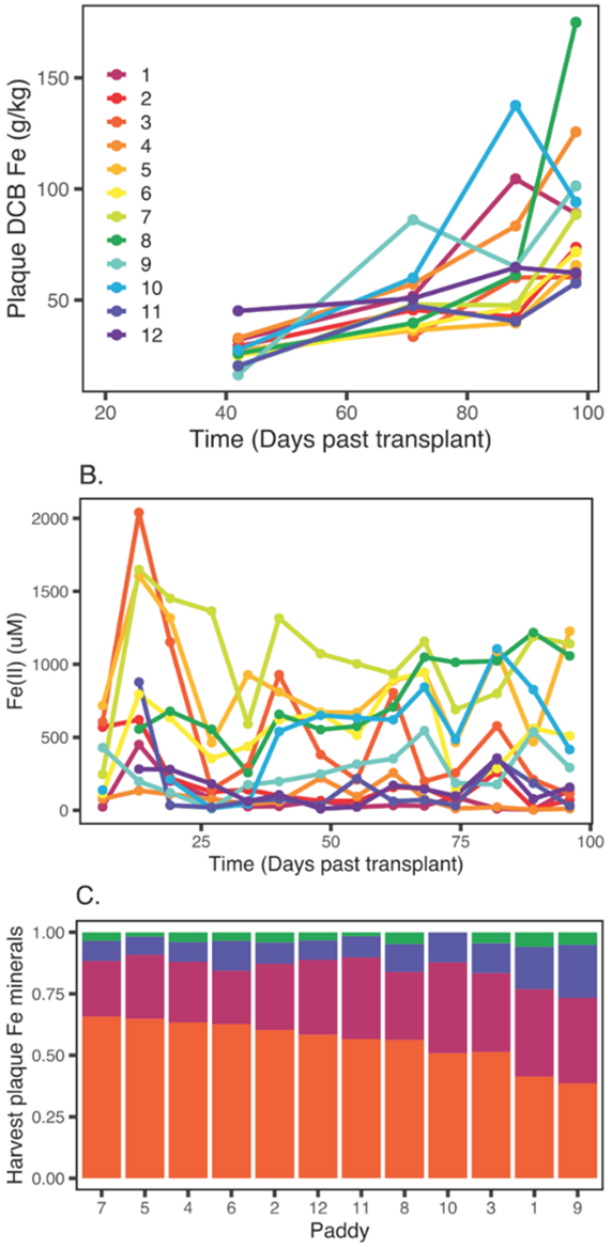

Figure 1. Plaque iron content compared to porewater Fe(II), and mineral composition. (A) Plaque iron content per dry root mass over the growing season plotted for 12 paddies sampled.

997 (B) Porewater Fe(II) over the growing season plotted by and colored by paddy (see legend in A).

998 (C) Plaque Fe mineral composition at harvest, by paddy, in order of decreasing ferrihydrite.

999

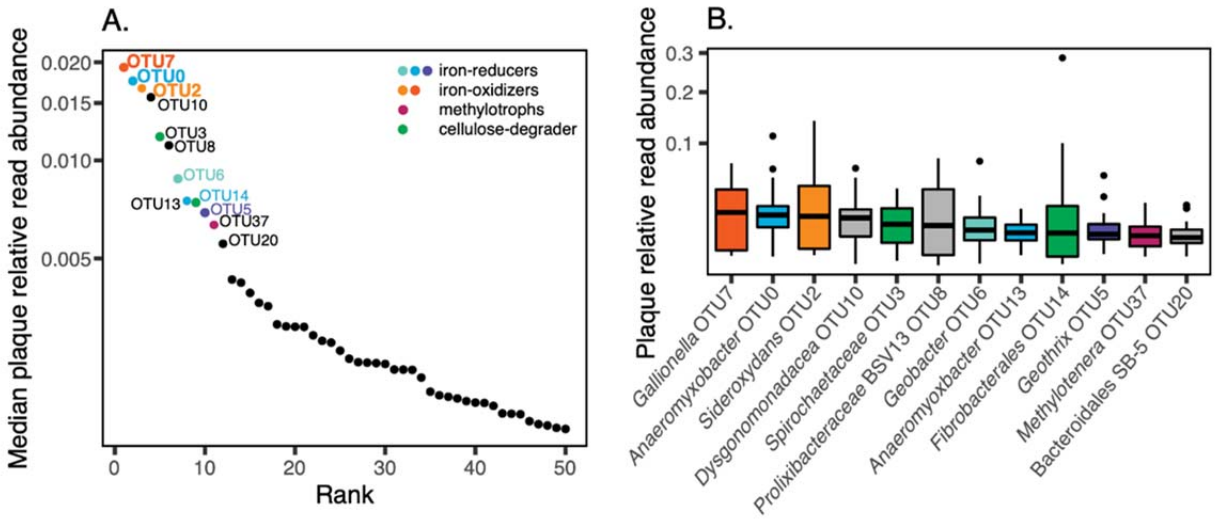

1000 **Figure 2. (**A) Log 10 median rank relative abundance curve of top 100 plaque organisms. (B)

1001 Box and whisker plot showing square-root transformed relative abundance of OTUs with median

1002 relative abundance above 0.5% in plaque. Boxes are colored according to known taxonomy with

1003 orange/yellow representing FeOB, pink/purple FeRB, blue methylotrophs, and green cellulose

1004 degraders. See Tables S1 and S2 for abundance data, ranking calculations, and taxonomic

1005 classification of OTUs.

A. Plaque

	Rank	Taxa	20 DPT	42 DPT	71 DPT	88 DPT	98 DPT
FeOB	1	*Gallionella* OTU7	0.85	1.4	4.2		8.0
	3	*Sideroxydans* OTU2	10	2.5	1.1		0.74
FeRB	2	*Anaeromyxobacter* OTU0	0.04	0.37	0.63		4.2
	7	*Geobacter* OTU6	0.13	0.71	12		0.71
	8	*Anaeromyxobacter* OTU13	0.38	1.3	1.4		1.1
	10	*Geothrix* OTU5	0.18	0.83	2.7		0.21

B. Rhizosphere

	Rank	Taxa	20 DPT	42 DPT	71 DPT	88 DPT	98 DPT
FeOB	1	*Gallionella* OTU7	2.0	4.8	2.5	2.0	3.4
	3	*Sideroxydans* OTU2	6.2	2.5	2.8	0.67	1.6
FeRB	2	*Anaeromyxobacter* OTU0	0.22	0.46	0.77	3.2	2.5
	7	*Geobacter* OTU6	0.39	0.42	1.1	0.62	1.2
	8	*Anaeromyxobacter* OTU13	0.59	1.6	1.3	1.5	1.3
	10	*Geothrix* OTU5	1.3	1.3	1.2	0.67	0.75

1006 **Figure 3.** Enrichment factors in plaque (A) and rhizosphere (B) of most abundant FeOB and
1007 FeRB OTUs over growing season (DPT=days past transplant). Enrichment factor was calculated
1008 as relative abundance in plaque or rhizosphere divided by relative abundance in bulk soil, and the
1009 median is given for each timepoint. Boxes are shaded according to enrichment factor, with those
1010 below 1 (not enriched) in white with gray text. (No plaque sample available for 88 DPT.) OTUs
1011 are ranked by median relative abundance in plaque.

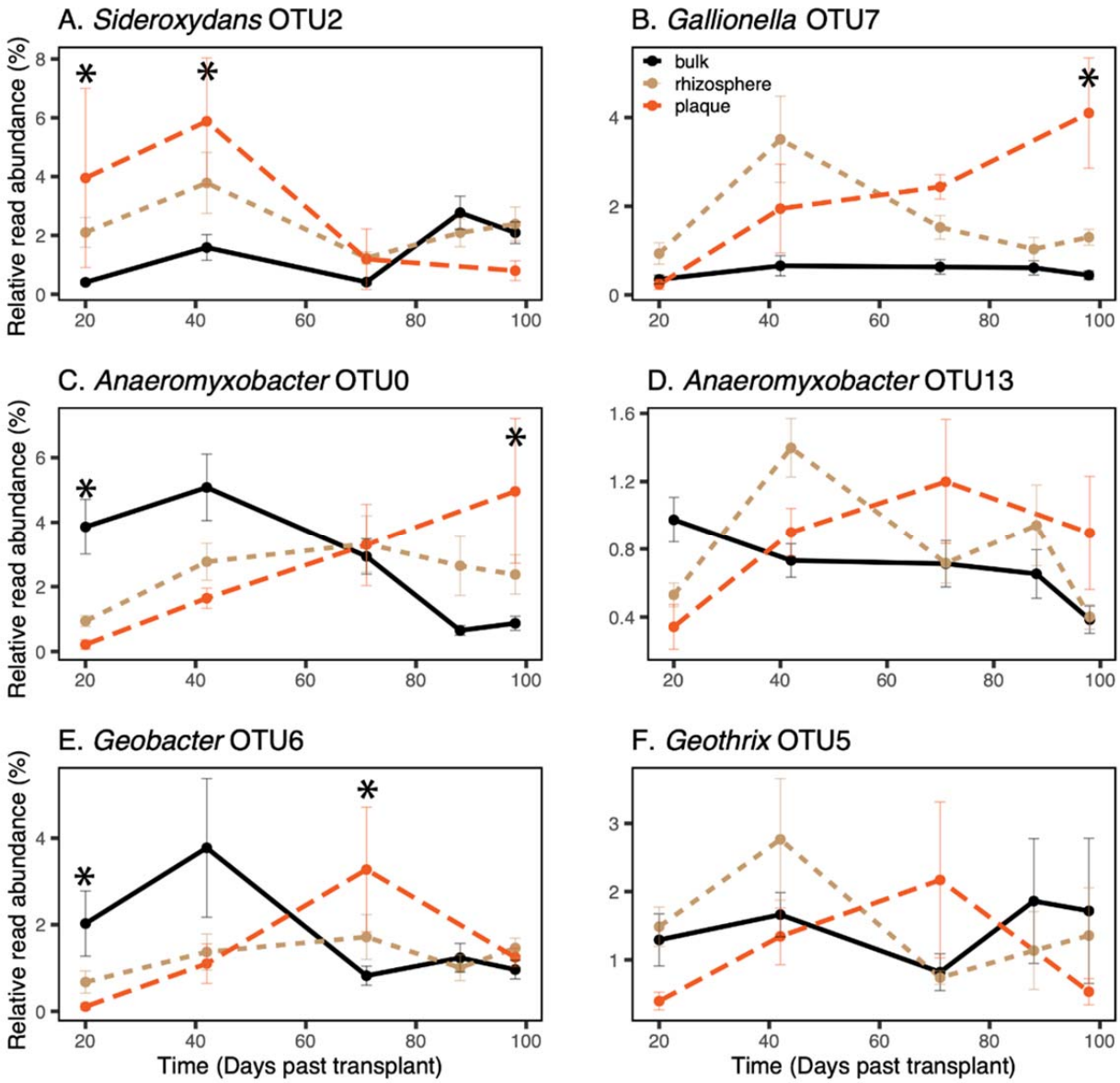

1012 **Figure 4.** Relative read abundance of top FeOB and FeRB in plaque (with median relative
1013 abundance above 0.5%) over time for each biosphere. Abundance in bulk soil plotted with black
1014 solid line, rhizosphere plotted in tan short-dashed line, and plaque plotted in orange long-dashed
1015 line. Error bars show standard error. Asterisks indicate differential abundance in the plaque and
1016 bulk soil where adj. p <0.1 based on DESeq2 analysis. Bulk 20 DPT n=12, rhizosphere 20 DPT
1017 n=12, plaque 20 DPT n=3, bulk 42 DPT n=11, rhizosphere 42 DPT n=10, plaque 42 DPT n=6,

bulk 71 DPT n=11, rhizosphere 71 DPT n=11, plaque 71 DPT n=4, bulk 88 DPT n=12, rhizosphere 88 DPT n=12, bulk 98 DPT n=11, rhizosphere 98 DPT n=11, plaque 98 DPT n=4.

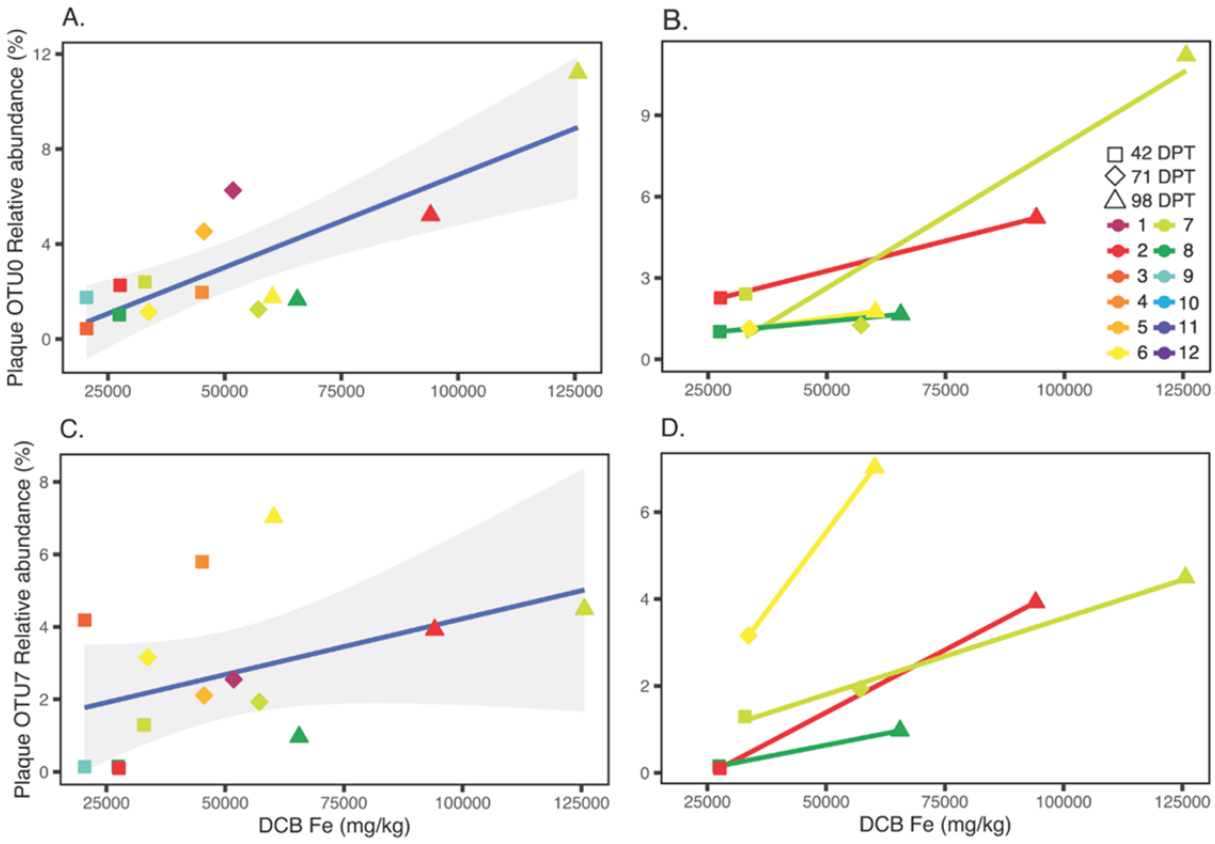

Figure 5. Comparison of selected FeRB and FeOB abundance with plaque iron content. Scatter plots show plaque relative abundance of *Anaeromyxobacter* OTU0 vs. plaque Fe (A, B), and of *Gallionella*/*Ferrigenium* OTU7 and plaque Fe (C, D). Points are colored by paddy and shapes represent sampling time (DPT). In A and C, all plaque data are shown and the blue line shows linear regression and gray shaded region shows 95% confidence interval. In B and D, only paddies with data from multiple time points are shown and temporal trends are plotted by paddy.

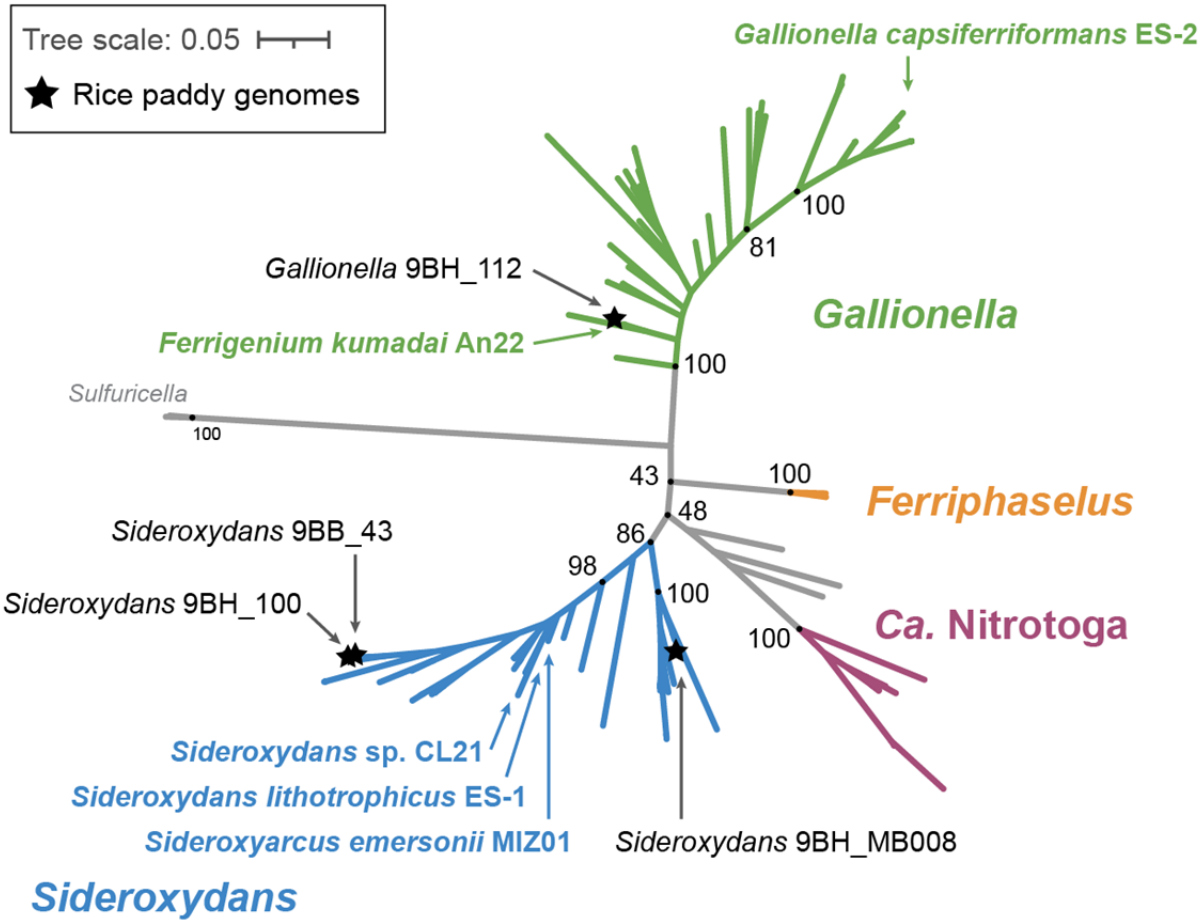

1027 **Figure 6.** Maximum likelihood tree of Gallionellaceae FeOB genomes based on 13 concatenated
1028 ribosomal protein sequences. Genomes from this study are shown with a star, and isolate
1029 genomes are shown by arrows only. While *Gallionella* 9BH_112 is closely related to the rice
1030 paddy isolate *F. kumadai* AN22, the other genomes in this study are more distant from isolates
1031 (in *Sideroxydans*). Support values based on 1000 bootstraps. Further information on
1032 classification and tree construction, including all genomes in the tree, are available in Hoover et
1033 al. (29).

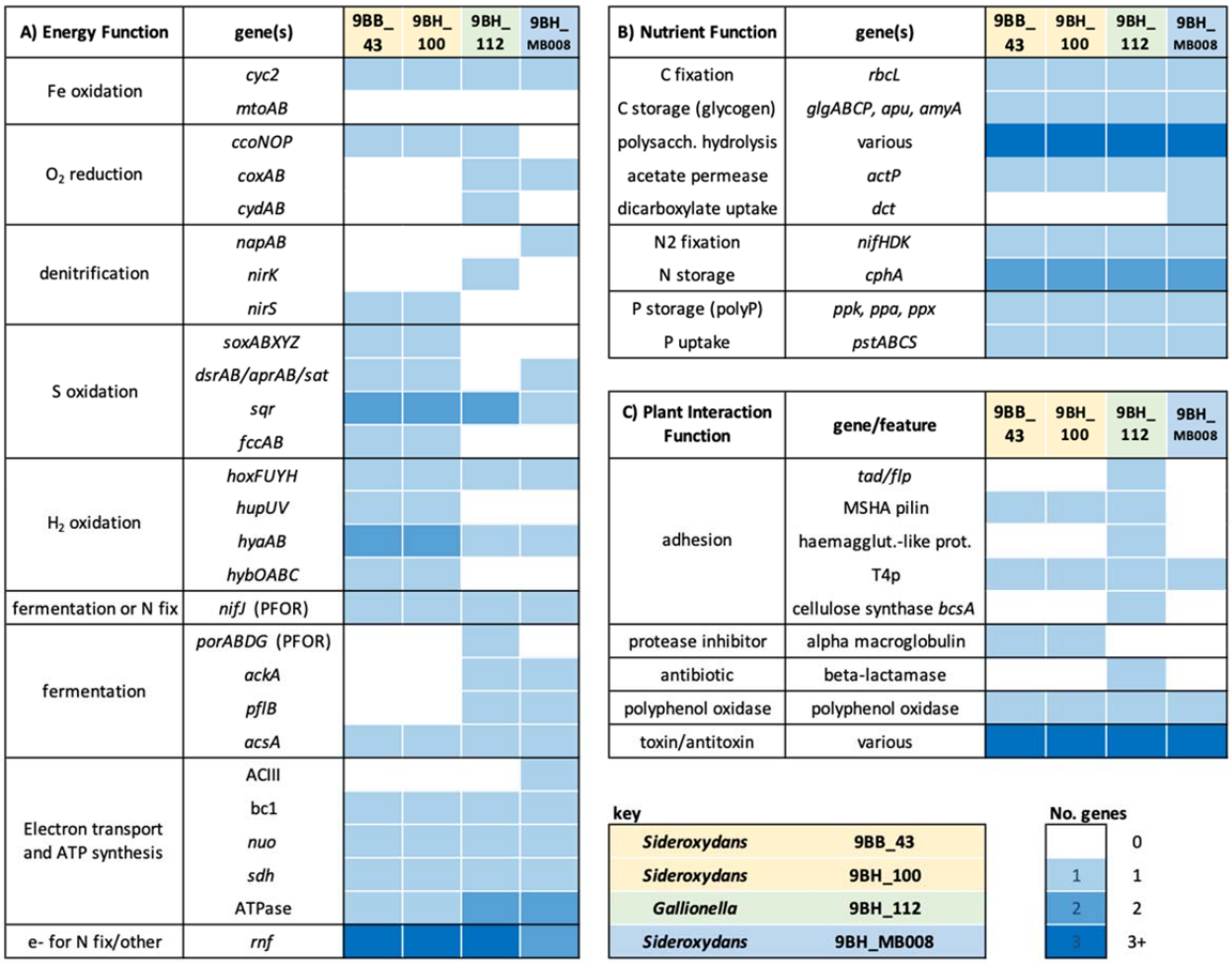

Figure 7. Summary of selected functional genes in Gallionellaceae FeOB genomes. Boxes are colored by number of genes ("No. genes") or gene sets (if >1 gene mentioned) present in each genome. See Table S4 for polysaccharide hydrolysis genes. "N fix" = nitrogen fixation.

FeOB or FeRB	Bin Name	Taxa	Complete-ness	Contamin-ation	Number of bases	No. contigs	%GC	16S
Fe-oxidizer	9BB_43	*Sideroxydans*	99.44	0	2,720,879	10	59.7	n
Fe-oxidizer	9BH_100	*Sideroxydans*	99.44	0	2,735,574	7	59.7	n
Fe-oxidizer	9BH_112	*Gallionella*	98.89	0.95	2,920,635	6	60.5	n
Fe-oxidizer	9BH_MB008	*Sideroxydans*	94.26	2.51	2,925,456	126	55.6	n
Fe-reducer	9BB_DT027	*Anaeromyxobacter*	98.06	0.65	4,302,736	312	75.3	y
Fe-reducer	9BB_IMG54	*Anaeromyxobacter*	93.55	3.51	4,148,843	177	72.5	n
Fe-reducer	9BH_IMG36	*Anaeromyxobacter*	96.82	0.35	4,208,782	273	72.8	y
Fe-reducer	9BH_DT025	*Anaeromyxobacter*	95.65	1.5	4,056,445	238	72.5	n
Fe-reducer	9BB_IMG16	*Geobacter*	100	0	3,353,205	6	51.0	n
Fe-reducer	9BB_IMG32	*Geobacter*	99.98	1.94	5,511,892	147	61.3	y
Fe-reducer	9BB_IMG87	*Geobacter daltonii*	98.67	2.58	3,912,958	78	55.9	y
Fe-reducer	9BH_IMG26	*Geobacterales*	99.32	1.29	3,710,533	39	52.2	n
Fe-reducer	9BH_DT005	*Rhodoferax*	96.21	4.09	5,701,076	665	57.8	n

1037 **Table 1. Metagenome-assembled genome bins**